Cooperative Strategies in the UWB TRPC Networks

by

Xue Dong

B.Eng., Harbin Institute of Technology, Harbin, China, 2008

A Thesis Submitted in Partial Fulfillment of the

Requirements for the Degree of

MASTER OF APPLIED SCIENCE

in the Department of Electrical and Computer Engineering

Cooperative Strategies in the UWB TRPC Networks

by

Xue Dong

B.Eng., Harbin Institute of Technology, Harbin, China, 2008

Supervisory Committee

Dr. Xiaodai Dong, Supervisor

(Department of Electrical and Computer Engineering)

Dr. Hong-Chuan Yang, Member

(Department of Electrical and Computer Engineering)

Supervisory Committee

Dr. Xiaodai Dong, Supervisor

(Department of Electrical and Computer Engineering)

Dr. Hong-Chuan Yang, Member

(Department of Electrical and Computer Engineering)

ABSTRACT

Transmitted reference pulse cluster (TRPC) was recently proposed for ultra-wideband (UWB) communications attributing to its robust performance, higher data rate, enhanced reliability and lower implementation complexity compared with the conventional transmitted reference technique. This thesis investigates the TRPC UWB relay strategies between two nodes lack of a direct link. Two novel channel quality indicators are first proposed for the TRPC UWB system, which can detect the channel condition and the relay decoding quality at the bit level without requiring estimating the channel state information. Five relay strategies based on these indicators (Relay Combining (RC), Weighted Relay Combining (WRC), Outage based Relay Selection (ORS), Maximum Product Relay Selection (MP-RS) and Minimax Relay Selection (MinMax-RS)) are proposed for the cooperative network to extend the network coverage and improve the system performance. The efficiency and effectiveness of the proposed cooperative strategies are examined under different channel environments through simulations, among which the MinMax-RS strategy based on the Log Likelihood Ratio (LLR) channel quality indicator is testified to yield the

best performance under the typical indoor line of sight (LOS) environment. Moreover, in order to reduce the relay overhead, a multipath channel based relay selection strategy (MC-RS) is proposed, where the channel quality is detected once for each channel realization and the noise variation in each bit is reasonably neglected. And base on both the channel and bit level selection, a joint relay selection (JRS) strategy is investigated to gain a balance between the channel condition and the bit-by-bit decoding quality at relays. At last, for the two-way-relay system prototype, the power allocation strategies are further investigated to minimize the system outage probability, under the limit of the total transmit power. Simulations in this thesis are executed under various channel environments following the IEEE 802.15.4a standard, and numerical results validate the effectiveness of the proposed strategies.

Contents

List of Tables

List of Figures

ACKNOWLEDGEMENTS

First and foremost I would like to thank my supervisor, Dr. Xiaodai Dong, for her valuable guidance, illuminating instructions, continuous encouragement and insightful technical advice throughout my study. This thesis could not have been completed without the generous support and help from Dr. Dong. I would also like to thank Dr. Hong-Chuan Yang, Dr. Jianping Pan for the valuable suggestions on revising my thesis. Thanks to many of my colleagues and friends at University of Victoria for being so nice and helpful, which makes my stay a great pleasure. Especially, I would like to thank Dr. Wei Xu, Dr. Zhonghua Liang, Yuzhe Yao, Le Chang, Mengting Wang, Tingy Zhao, Rongrong Zhang, Li Jin, Yuanqian Luo, Guowei Zhang, Siyuan Xiang, Zhe Yang, Chris Liu, Shuai He, Congzhi Liu, GuangYu Wang, Jimmy Tian for their priceless help. Special thanks to Erik, Steve, Vicky, Moneca, Don Mai and for the many patience and constant help. Lastly, I would like to thank my father, for his love, understanding, constant support, and most of all, his confidence in me and my abilities. A million words would be too short for my gratitude and I will just say, I love you, Dad. And to my most rememberable Mom, I will cherish the every single day you were with dad and me, and you will always live in my heart!

Xue Dong

DEDICATION

To my parents!

Chapter 1

Introduction

As one of the booming technologies in wireless communication nowadays, Ultra wideband (UWB) is defined either as a signal with its fractional bandwidth exceeding 20% of the center frequency or its instantaneous bandwidth greater than 500 MHz according to [3] [4]. And its operations can be classified into three separate categories as: communication and measurement systems, vehicular radar and imaging systems (including the ground penetrating radar, through-wall imaging and surveillance systems), and medical imaging systems; each of these categories is allocated a specific spectral mask [4]. As a result of the huge potential in UWB applications, this thesis aims at investigating the the relay selection and power allocation strategies for the UWB networks.

In this chapter, a brief overview of the UWB technology is first presented, followed by the description of two important issues related to classifications of UWB signals and the cooperative communication in UWB relay networks. In Section 1.1, the background of the UWB technology is introduced. In Section 1.2, a brief introduction towards the classifications of UWB signals and the corresponding transceiver design are presented. The fundamentals of the two-way-relay network structures are

described in Section 1.3. Finally, the organization of the thesis is explained at the end of this chapter.

1.1 Background of UWB Technology

Ultra Wideband (UWB) communication systems can be broadly classified as any communication system whose instantaneous bandwidth is many times greater than the minimum required to deliver particular information. This excess bandwidth is the defining characteristic of UWB. In February 2002, the FCC regulation limits the radiation power of indoor communication UWB systems to less than -41.3 dBm/MHz within 3.1-10.6 GHz [3], as shown in Fig. 1.1. While the newly published Canadian

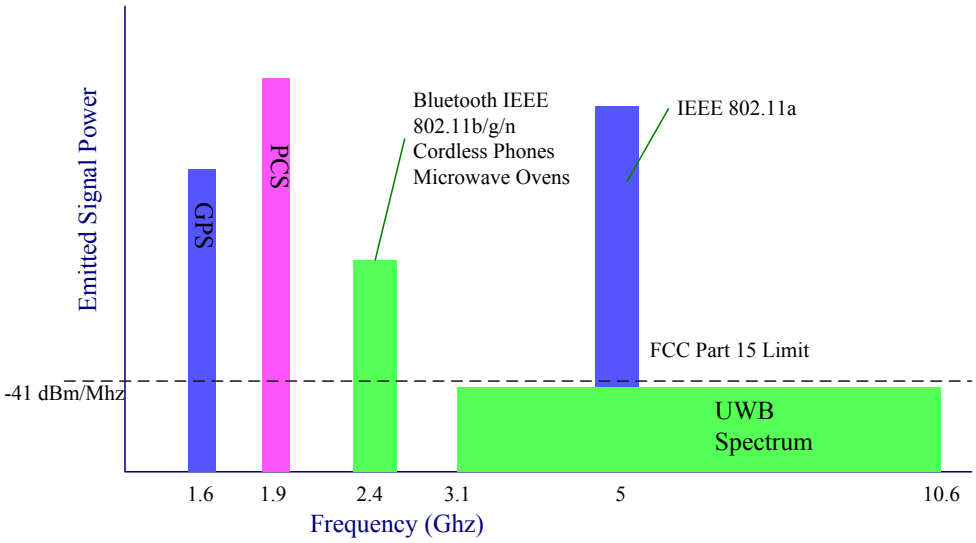

Figure 1.1: Designated UWB spectrum and other higher-power narrowband systems

UWB regulation limits the equivalent isotropically radiated power (EIRP) to -70 dBm/MHz in the frequency range of 1.61-4.75 GHz, and -41.3 dBm/MHz from 6 GHz to 10.6 GHz [4]. The regulatory allocations are intended to provide an efficient use of the scarce radio bandwidth, while enabling both the high data rate wireless

connectivity (e.g.,the personal area network (PAN)) and longer-range, low data rate applications (e.g., radar and imaging systems) at the same time. Such strict restrictions avoid interference to legacy (narrowband) systems, which means operating under these regulations will not disturb any of the existing narrowband system at all and can assure the narrowband systems operate properly.

The UWB systems have the following characteristic compared with the conventional narrowband ones [5], as:

1. Large instantaneous bandwidth enables fine time resolution for network time distribution, precision location capability, and use as a radar.

2. Short duration pulses are able to provide robust performance in dense multipath environments by exploiting more resolvable paths.

3. Low power spectral density allows coexistence with existing users and has a low probability of intercept.

4. Data rate may be traded for power spectral density and multipath performance.

These features of UWB promise it highly potential in various applications. Due to the short duration of the UWB pulses, it is easier to engineer extremely high data rates, and the data rate can be readily traded for range by simply aggregating pulse energy per bit using either simple integration or coding techniques. Furthermore, the Orthogonal Frequency-Division Multiplexing (OFDM) technology can be adopted in UWB, subject to the minimum bandwidth requirement of the regulations. On the other hand, by using a large portion of the radio spectrum, UWB can be operated at very low energy level. Therefore, the precision capabilities combined with the very low power operation make the UWB systems ideal for certain radio frequency sensitive environments such as hospitals and healthcare. Moreover, UWB is also being used

in the "see-through-the-wall" precision radar imaging, radio based precision locating and tracking, and precision time-of-arrival-based localization [6].

In all, what makes UWB systems unique is its instantaneous bandwidth and the potential for very simple implementations. Additionally, the large bandwidth and potential for low-cost digital design enable a single system to operate in different modes as a communication device, radar, or locator. Taken together, these properties give UWB systems a clear technical advantage over any other conventional technologies in high multipath environments at low to medium data rates.

1.2 Transmitted Reference based UWB Communications

1.2.1 Classifications of UWB Signals

The UWB technique is usually divided into two classes: one is to convey information through sending pulses with very short duration, namely the Impulse UWB (I-UWB); and the other approach using multiple simultaneous carriers is called Multicarrier UWB (MC-UWB).

Orthogonal Frequency-Division Multiplexing is the most typical realization of MC-UWB. It is particularly well-suited for avoiding interference, because its carrier frequencies can be precisely chosen to avoid collisions with narrowband systems. Moreover, it is more flexible and scalable. However, the high-speed Fast Fourier Transform (FFT) processing is indispensable in OFDM, which requires massive processing powers. Thus the implementing of a MC-UWB front-end is challenging, because the power is continuously changing over a very wide bandwidth.

On the other hand, the transmit signal of I-UWB is a series of extremely short

baseband pulses, unlike the traditional communication techniques which use a modulated sinusoidal carrier to convey information [7]. Attributing to its architecture simplicity and that it is very inexpensive to build, the I-UWB system will be adopted for the rest of this thesis.

1.2.2 I-UWB Transceiver Design

The I-UWB receivers can be broadly categorized as the threshold or leading edge detectors (LED), RAKE receivers and correlation detectors (CD). The advantages and disadvantages of the three types of I-UWB receivers can be briefly described as follows:

Leading Edge Detector : The LED is some of the earliest and simplest of all I-UWB receivers [8]. It works by setting a threshold at the receiver, and any incoming pulse that crosses the threshold is detected and demodulated. The advantage of a LED receiver lies in the simplicity of implementation. However, it has drawback in that it is susceptible to noise spikes and is incapable of taking advantages of multipath signals, which is a significant character of the UWB channel.

Rake Receiver : The RAKE receiver can be used in any kind of spread spectrum communication systems to accumulate energy in the significant multipath components. It can ideally reject out self-interference resulting from the multipath effects, as well as other forms of interference like multiaccess interference and adjacent channel interference. However, there are four major drawbacks in the I-UWB RAKE receiver design. First of all, the energy capture is relatively low for RAKE receiver with a moderate number of fingers when Gaussian pulses are used [7]. Secondly, as each multipath undergoes a different channel, distor-

tion is introduced in the received pulse shape, and it makes the use of a single line-of-sight(LOS) path signal becoming a suboptimal template. Third, channel estimation is critical in RAKE receivers for the maximum ratio combining (MRC), thus an imperfect channel estimation will easily lead to the degradation of system performance. Last, the synchronization (acquisition and tracking) is hard to realize for pulses within subnanosecond duration. As a result, the design of the I-UWB RAKE receiver is highly impractical.

Correlation Detector : The CD is also known as a matched filter receiver. It has advantage that the correlation operation can be done in either analog or digital circuits, while the primary disadvantage attributes to the imperfect correlations from distortion in input pulses.

Different modulation techniques may be adopted in an I-UWB transceiver, e.g., the modulation techniques may involve time-hopped pulse position modulation (TH-PPM), time-hopped antipodal pulse amplitude modulation (TH-A-PAM), optical orthogonal coded pulse position modulation (OOC-PPM), direct sequence spread spectrum modulation (DS-SS), transmitted reference (TR), and etc. And the background of the TR system with an autocorrelation receiver is introduced in the next subsection.

1.2.3 Preliminary Description of the TR System

The fine time solution of I-UWB signals results in the channel being extremely frequency selective, and also leads to a significant number of resolvable multipath components at the receiver. Thus, the requirement for a receiver structure raises in order to achieve maximum energy capture. However, an alternative approach is to adopt an autocorrelation receiver, which correlates the current received signal with a previous received signal. For example, a transmitted reference (TR) system applies autocorre-

lation detection [1]. The TR system does not require explicitly estimating the dense multipath UWB channels, and collects the channel energy more easily compared to a coherent Rake receiver [9]. Moreover, the frequency dependent effects of a UWB channel are taken into account directly in the TR scheme.

As mentioned before, due to the strict low transmission power requirement posed by FCC, UWB signals have to act like background noise to the existing communication systems. To increase the effective signal-to-noise ratio (SNR) and obtain a reasonable error performance in the UWB system, one bit waveform is usually designed to transmit repeatedly over multiple frames in a symbol duration. Instead of repeating a single data pulse, the TR frame in a TR system contains a pulse pair, i.e., reference (unmodulated) pulse and data (modulated) pulse.

For simplicity, let's assume the UWB channel is slowly varying, and remaining unchanged during the period of the reference and data pulse pairs transmission. By sending the reference pulse with known polarity, the demodulation is carried out by a simple delay-and-multiply procedure, which essentially correlates the received reference and data pulses, and extracts the data bit accordingly. To ensure the reference and data pulse will not overlap after going through the multipath channel, the TR transmitter requires that the interval between the reference and data pulses within a frame be longer than the channel impulse response. Because the delay line in the delay-and-multiply procedure of the TR receiver must match the interval between the reference and data pulses, there is an underlying requirement that the TR receiver must be able to implement accurate analog delay lines which are longer than the UWB channel impulse response.

Based on the structure of the TR system, a delay hopped TR (DHTR) system was first proposed in [10]. And the performance analysis of a TR system was carried out in [11]-[12]. A variation to this original TR scheme employing antipodal

modulation was presented in [13], and simulation results revealed that the proposed detection schemes provide significant performance improvements in terms of bit error rate (BER) over the conventional TR receiver structure.

However, as of today, implementing an analog delay line longer than 10 ns is beyond the industrial capability [11], whereas most UWB channels are longer than 20 ns. Therefore, designing a TR receiver in the real world can be very challenging. A more implementable transceiver structure, namely transmitted reference pulse cluster (TRPC), is proposed in [1] accordingly. Different from the conventional TR structure, TRPC pushes the reference and data pulses close together and makes the delay line as short as the pulse width. This makes the implementation of a transmitter feasible, since it only requires a very short analog delay line. Although the inter-pulse interference (IPI) is expected in the TRPC structure due to its compact nature, the evenly spaced pulse pattern and the unique detection method compensate the performance loss, and show a substantial performance gain compared with conventional TR detection. The selection of integration interval for TRPC systems is extensively investigated in [14].

As the TRPC structure enables a low complexity, robust and practical autocorrelation detector to be used at the receiver, the rest of the thesis is based on this structure.

1.3 UWB Relay Networking

1.3.1 Introduction of Cooperative Communication

The idea of relay is first proposed by Shannon's two-way channel (TWC). According to [15], a two-way channel has two terminals, each of them attempting to get across a message to the other terminal. The sources that generate the messages are assumed

to be independent.

The concept of the cooperative communication today is evolved from the TWC prototype. In modern wireless networks, signal fading arising from multipath propagations is a severe channel impairment, but it can be mitigated through the use of diversity. Thus, space or multiple-antenna diversity techniques are particularly attractive as they can be readily combined with other forms of diversity (e.g., time and frequency diversity), and still offer dramatic performance gains when other forms of diversity are unavailable. In contrast to space diversity using the forms of physical arrays, cooperative network is built upon the classical relay channel model, and exploits space diversity using a collection of distributed antennas belonging to multiple terminals [16]; thus it is drawing increasing attention nowadays. This class of methods is called cooperative communication, and it enables single antenna mobiles to share their antennas in a multi-user environment and generates a virtual multiple-antenna transmitter that allows them to achieve transmit diversity [17].

A classic system model for the cooperative communication can be found in [18]. And based on this relay structure, three cooperative signaling modes are universally adopted nowadays, namely the amplify and forward (AF) method, coded cooperation and decode and forward (DF) method.

Amplify and Forward : According to the AF method, relay receives a noisy version of the signal transmitted by its partner first, and then amplifies and retransmits it. Although noise is amplified through the cooperation, the recipient receives two independently faded versions of the signal; hence better decisions can be made for the detection. The problem of the AF mode is that the sampling, amplifying, and retransmitting of analog values is technologically nontrivial.

Coded Cooperation : Coded cooperation is a method that integrates cooperation into channel coding. It works by sending different portions of the source's code

words via two independent fading paths. The reason why coded cooperation has high efficiency is that the whole procedure is managed automatically through code design, with no feedback between the users.

Decode and Forward : In the DF method, relay attempts to detect and retransmits the detected bits. Note that the cooperation is not always beneficial, it is possible that the dection will be in error, which will cause false detection at the destination. The whole process leads to the problem of error propagations. However, this signaling has the advantage of simplicity, and it is more adaptable to channel conditions. Therefore, DF is adopted as the signaling method in the rest of this thesis.

Different relaying schemes have been investigated when there are multiple relays in the cooperative network. In [19], an opportunistic relaying scheme that alleviates the demand of the assumptions of central scheduling and channel state information (CSI) at transmitters is proposed. The key idea is to allocate each hop with only a subset of nodes that can benefit from the multiuser diversity. To select the source and destination nodes for each hop, relays operate independently with the CSI at receiver only, and return an index-valued feedback to the transmitter. Relay selection strategies are investigated under both DF and AF schemes in [20]. The findings reveal that cooperation can offer diversity benefits even when cooperative relays do not choose to transmit, but rather to cooperatively listen. That is to say, they only act as passive relays and give priority to the transmission of a single opportunistic relay.

1.3.2 Physical Layer Network Coding (PNC)

In a two-way-relay channel (TWRC), defined as the bidirectional transmission between two end nodes with relay nodes in between, network coding can be applied at the relay node to exploit the broadcast nature of the wireless medium.

In traditional networks, interference can be avoided by prohibiting the overlapping of signals from node 1 (represented by N_1 for short) and N_3 to N_2 in the same time slot. A possible transmission schedule is given in Fig. 1.2. Let S_i (i=1, 3) denote the information initiated by N_i, then N_1 first sends S_1 to N_2, and then N_2 relays the decoded $\hat{S}_1$ to N_3. After that, N_3 sends S_3 via N_2 in the reverse direction. A total of four time slots are needed for the exchange of two frames in opposite directions.

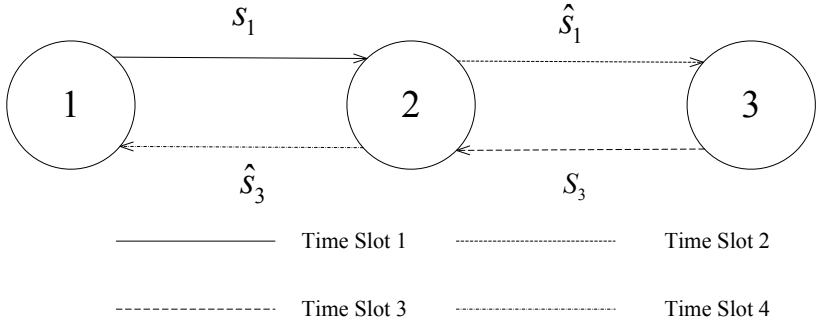

Figure 1.2: Traditional scheduling scheme

The idea of PNC is firstly proposed in [21]. Furthermore, with the help of the Repeat Accumulate (RA) channel code, the system performance can be significantly improved in terms of BER without adding complexity [22]. In [23], an estimate and forward (EF) strategy was proposed to minimize the average probability of error in a TWRC via functional analysis.

Fig. 1.3 illustrates the idea of Physical Layer Network Coding (PNC). At first, N_1 sends S_1 to N_2 and then, in the second time slot, N_3 sends S_3 to N_2. After receiving

S_1 and S_3, N_2 encodes information S_2 as follows:

$$S_2 = \hat{S}_1 \oplus \hat{S}_3 \tag{1.1}$$

where $\oplus$ denotes the bitwise exclusive "OR" operation applied over $\hat{S}_1$ and $\hat{S}_3$. N_2 then broadcasts S_2 to both N_1 and N_3. When N_1 receives S_2, it extracts S_3 from $\hat{S}_2$ using its local information S_1, as follows:

$$S_1 \oplus S_2 = S_1 \oplus (S_1 \oplus S_3) = S_3. \tag{1.2}$$

Similarly, N_2 can extract S_1. A total number of three time slots are needed, gaining a 25% improvement in the throughput over the traditional transmission scheduling scheme.

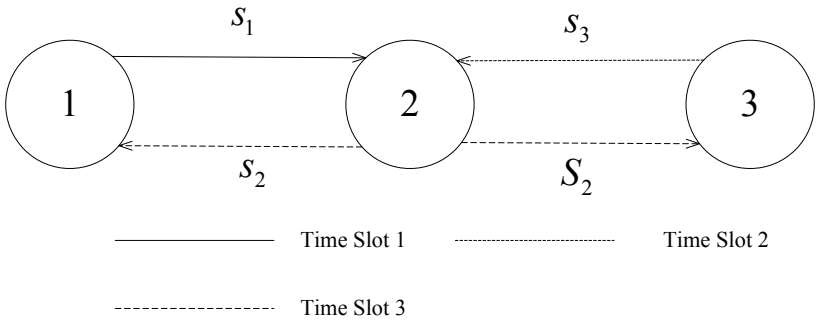

Figure 1.3: Physical Layer Network coding scheme

The physical layer network coding is executed under the DF signaling mode, and there is another approach of the network coding, which is named as analog network coding (ANC) [24]. ANC is essentially a form of linear self-interference cancelation with the use of a-priori known information. The AF method should be adopted as the signaling mode if ANC is executed at the relay, and hence the interference is inevitable between the source nodes. In order to cancel self-interference, the knowledge of

full channel state information is required, which is difficult to obtain for frequency selective UWB channels, thus PNC is adopted as the relay coding scheme in this thesis.

1.3.3 Cooperation in UWB

As it has been mentioned above, UWB is a short range communication technology. A primary application of UWB is the high rate Wireless Personal Area Network (WPAN) confined to a small coverage area (less than 10 m radius). The network should be a self-organized, dynamic ad hoc network, which means the network is formed without advanced planning, and users can join or leave at any time. However, through the use of cooperative relays, such a network can extend its coverage, or data rate performance.

Previous work on cooperative UWB communication systems can be found in [25]-[26]. A general construction technique of distributed Space Time (ST) coding for the AF cooperative scheme is presented in [25], where the totally-real codes are well suited for low complexity, carrierless UWB cooperative systems. In [26], two families of efficient distributed cooperative data relaying schemes are developed and investigated, which can be adopted to forward data within an I-UWB ad-hoc network, namely the distributed cooperative routing schemes and distributed cooperative beamforming schemes. Performance analysis and simulation studies show the effectiveness and efficiency of the two proposed schemes. Optimized modulation schemes combined with the network coding are investigated in [27]. However, to the author's best knowledge, there is little study on two-way-relay UWB networks in the literature, which is the topic of this thesis.

1.4 Agenda

The major focus of this thesis is to propose and intensively investigate the effective relaying strategies in the UWB networks. Different TRPC cooperative strategies are proposed for a bi-directional two relays UWB network, via physical layer network coding. For a fair comparison, the system is set to have the same data rate for each strategy. We introduce two novel decision variable (DV) based channel quality indicators, which are used to estimate the channel conditions and decoding qualities at relays. Then relay selection strategies based on these indictors are proposed and demonstrated to achieve improved performance over directly combining decision variables from the two relays. Additionally, to reduce the relay overhead, a multipath channel based relay selection method is introduced, which chooses the cooperative relay once for each channel realization instead of the bit level. Moreover, a joint relay selection strategy combining both the bit-by-bit and multipath channel based relay selection is proposed, this method provides a balance on the system performance and hardware complexity. Furthermore, for the two-way-relay prototype, the optimization method for minimizing the system outage probability is investigated, limited by the total transmit power.

The thesis is organized as follows:

Chapter 2 : outlines the UWB communication system. At the beginning, a brief introduction is given on IEEE 802.15.4a channel modeling. As a background review, the TRPC structure is presented, and the performance of the TRPC is summarized for zero and adaptive threshold respectively. Then the two-way-relay channel is introduced, followed by the cooperative network structure adopted in this thesis.

Chapter 3 : proposes two decision variable based channel quality indicators, one is

based on the distance of the DV to the decision threshold, normalized by the distance between the noiseless DV and the decision threshold; and the other is based on the log likelihood ratio (LLR). They are both demonstrated to reflect the channel condition as well as the decoding quality, without requiring estimating the UWB channel state information. Five cooperative relay strategies based on these indicators are then proposed, and they are examined through the theoretical analysis and numerical simulations. The numerical BER results verify the analytical formulations, and all the proposed cooperative strategies are proved to be more reliable than the scenario that directly combins DVs from two relays, among which the MinMax Relay Selection (MinMax-RS) strategy yields the most robust performance.

Chapter 4 : investigates the cooperative networks under severe shadowing environment. For the CM1 channel environments, simulations are taken for the cooperative strategies proposed in Chapter 3 when shadowing effects are considered in different hops of the network. For the highly dispersive environment under the CM8 channel model, where shadowing effect becomes significant, a novel multipath channel based relay selection strategy is proposed to reduce the system overhead. Then a joint relay selection strategy combining both multipath channel based selection and bit-by-bit detection is investigated. The joint relay selection strategy can reduce the relay overhead, while still has its performance approaching that of the channel quality indicator based cooperative strategies.

Chapter 5 : focuses on a three nodes two-way-relay system, with the assumption that the second user roaming around the relay. The power allocation strategy is investigated to minimize the outage probability for such a system. The probability density function (PDF) on SNR for a single hop UWB TRPC realization

is built through Monte Carlo methods first, followed by an approximated outage probability function for the cooperative network. An optimized power allocation algorithm is further proposed to the minimize the system outage probability. Extensive simulation indicates that the proposed optimization method outperforms other power allocation schemes.

Chapter 6 : concludes the thesis and proposes the future work.

Chapter 2

UWB TRPC System Model

2.1 IEEE 802.15.4a Channel Model

In wireless communication systems, the received signal is an attenuated, delayed, and possibly distorted version of the transmitted signal plus noise. The relationship between the received signal and the transmitted signal is typically defined as the "channel". Given the very wideband nature of UWB signals (i.e., up to tens of GHz in the frequency bandwidth), the conventional channel models developed for narrowband transmissions are inadequate for the UWB transmission.

Traditional channel models for path loss assume that diffraction coefficients, attenuation due to materials, and other propagation effects are constant over the band of interest. When the fractional bandwidth [1] is 0.01 or less, this is a safe assumption. Additionally, narrowband models often incorporate antenna effects (such as the effective aperture) into path loss. Again, this is acceptable only when the change in these antenna effects is negligible over the bandwidth. However, neither of these assumptions is correct for a UWB system.

[1] The formula proposed by the FCC commission for calculating the fractional bandwidth is $2(f_H - f_L)/(f_H + f_L)$, where f_H represents the upper frequency of the -10dB emission limit and f_L represents the lower frequency of the -10dB frequency limit.

One of the most important features of the wireless channel is fading, which refers to fluctuations in the envelop of a transmitted radio signal. The UWB channel can be modeled by large scale fading, shadowing (or medium scale fading), and small scale fading. The definition of these three fadings are as follows:

Large Scale Fading: the gradual loss of the received signal power with transmitter-receiver separation is referred to as large scale fading. It is averaged over time and a sufficiently large spatial area.

Medium Scale Fading or Shadowing: the random variation of the signal due to peculiarities of the particular environment surrounding the transmitter and receiver. Shadowing happens at a faster time scale compared to large scale fading, but slower than small scale fading.

Small Scale Fading: the signal fluctuates over very small distances which is in the order of several wavelength. It is caused by the constructive or destructive superposition of unresolvable multipaths.

The generic IEEE 802.15.4a channel model [28] adopts the Saleh-Valenzuela (SV) [29] shape and is used for the 100-1000 MHz and 2-10 GHz channel model. It is the physical realization of the multipath components arriving in clusters, and has its impulse response represented by

$$h_{discr}(t) = \sum_{l=0}^{L} \sum_{k=0}^{K} a_{k,l} \exp(j\phi_{k,l}) \delta(t - T_l - \tau_{k,l}). \tag{2.1}$$

where $a_{k,l}$ and $\phi_{k,l}$ are the tap weight and the phase of the k-th ray in the l-th cluster, respectively; and $\phi_{k,l}$ is uniformly distributed over the range $[0, 2\pi]$. L is the number of the clusters which follows Poisson distribution as

$$pdf_L(L) = \frac{(\bar{L})^L \exp(-\bar{L})}{L!}. \tag{2.2}$$

where the mean $\bar{L}$ completely characterizes the distribution.

The cluster arrivals are described as a Poisson process with mean arrival rate Λ_l (assumed to be independent of l). Within each cluster, the component arrivals are also described as a Poisson process with parameter λ, where $\lambda \gg \Lambda$. The arrival time of the l-th cluster is denoted by T_l, and the arrival time of the k-th component within the l-th cluster is denoted by $\tau_{k,l}$. Then according to the model, there is

$$p(T_l|T_{l-1}) = \Lambda_l \exp\left[-\Lambda_l(T_l - T_{l-1})\right], \quad l > 0 \tag{2.3}$$

$$p(\tau_{k,l}|\tau_{k-1,l}) = \lambda \exp\left[-\lambda(\tau_{k,l} - \tau_{k-1,l})\right], \quad k > 0. \tag{2.4}$$

Due to the discrepancy in the fitting for different indoor and outdoor scenarios, the arrival time of multipath components given by (2.4) is updated with a mixture of two Poisson processes [28] as

$$p(\tau_{k,l}|\tau_{k-1,l}) = \beta\lambda_1 \exp\left[-\lambda_1(\tau_{k,l} - \tau_{k-1,l})\right] + (1-\beta)\lambda_2 \exp\left[-\lambda_2(\tau_{k,l} - \tau_{k-1,l})\right], \quad k > 0, \tag{2.5}$$

where β is the mixture probability, and λ_1 and λ_2 are the ray arrival rates.

The cluster energy decays exponentially, therefore the average power of the l-th cluster Ω_l is given by

$$10\log\Omega_l = 10\log\left(\exp(-T_l/\Gamma)\right) + M_{cluster}, \tag{2.6}$$

where Γ is the cluster exponential decay factor and $M_{cluster}$ is a normally distributed variable with standard deviation $\sigma_{cluster}$ around it.

Similar to the inter-cluster situation, the mean power of the k-th multipath com-

ponent within the l-th cluster also decays exponentially, and can be represented by

$$\Omega_{k,l} = \frac{\Omega_l}{\gamma_l \left[(1-\beta)\lambda_1 + \beta\lambda_2 + 1\right]} \exp\left(-\tau_{k,l}/\gamma_l\right), \tag{2.7}$$

where Ω_l is the integrated energy of the l-th cluster given by (2.6), and γ_l is the component exponential decay factor.

For the non-line-of-sight (NLOS) scenarios under certain environments (office and industrial), where the reflection of the signal might result in larger received energy, the shape of the power delay profile does not follow the exponential decay as in (2.7). Instead, it has a distribution with a rising period followed by decay, as

$$\Omega_{k,l} = \left(1 - \chi \exp(-\tau_{k,l} - \gamma_{rise})\right) \cdot \left(-\tau_{k,l}/\gamma_1\right) \cdot \frac{\gamma_1 + \gamma_{rise}}{\gamma_1} \cdot \frac{\Omega_l}{\gamma_1 + \gamma_{rise}(1-\chi)}, \tag{2.8}$$

where parameter χ describes the attenuation of the first ray, γ_{rise} represents how fast the power delay profile increases to its local maximum, and γ_1 determines the decay at late times.

Besides the power delay profile is derived, the small scale fading is modeled as Nakagami distributed [30], thus the weight of the tapped delay $a_{k,l}$ follows the distribution

$$pdf_{a_{k,l}}(a) = \frac{2}{\Gamma(m)} \left(\frac{m}{\Omega_{k,l}}\right)^m a^{2m-1} \exp\left(-\frac{m}{\Omega_{k,l}} a^2\right), \tag{2.9}$$

where parameter m is modeled as a lognormally distributed random variable with logarithm mean μ_m and standard deviation σ_m, and $\Omega_{k,l}$ is given by (2.7) or (2.8), depending on the specific scenarios.

The specification above lays out the basic UWB channel model. In the prototype codes provided within [28], 8 different environments are modeled with complete sets of parameters. However, although suitable for the simulation, the generic model is

very complicated for analytical derivation. Therefore, all the analysis done towards the UWB channels are based on the tapped delay model instead, which generalizes the channel as a simple tapped delay lines as

$$h(t) = \sum_{k=0}^{K-1} \alpha_k \delta(t - \tau_k) \tag{2.10}$$

where α_k and τ_k are the complex amplitude and delay of the k-th multipath.

2.2 Transmitted Reference Pulse Cluster (TRPC) System in UWB Communications

According to the demodulation schemes, I-UWB receivers can be generally categorized into the coherent receiver and non-coherent receiver. The coherent scheme needs precise timing synchronization as well as accurate channel estimation, which makes it quite complex; while the non-coherent scheme is much simpler but has to sacrifice the performance. Trade-offs must be made in the receiver design in order to balance between complexity and performance.

An I-UWB system undergoes ample multipaths due to its inherent high time resolution. However, to fully take advantage of the multipath components for diversity and robustness, a highly complex coherent receiver is needed. That means not only stringent synchronization and accurate channel estimation are needed, but an ultra-fast analog to digital converter (ADC) and a digital signal processor with extremely high performance should be considered as well. Thus, alternative receiver structures based on non-coherent techniques are drawing increasing attention.

Non-coherent receivers are able to recover the energy spreading in the multipath channels without requiring channel estimation. However, in the conventional TR

systems, there are two major drawbacks, one is the long delay line which is physically unrealizable, and the other is the 3 dB power loss caused by transmitting non-databearing reference pulses.

A new transmitted reference pulse cluster (TRPC) structure is thus proposed to meet the implementation constraint of long delay lines that conventional TR systems have to face; moreover, it outperforms the conventional TR significantly [1]. Unlike conventional TR, TRPC places reference pulse and data modulated pulse back to back, which is called a dual pulse. And several dual pulses are placed together without space between them to compose a pulse cluster.

2.2.1 Preliminary Description of TRPC System

The transmitted reference pulse cluster is composed of an even number ($2N_f$) of uniformly and closely spaced pulses, where all the even-numbered pulses have the same polarity and so do the odd-numbered pulses. If the antipodal signaling is adopted, the relative polarity between even and odd-numbered pulses represents the information data. The pulse structure of a TRPC system is shown in Fig. 2.1, where T_s is the symbol duration determined by the bit rate.

The m-th TRPC transmit signal can be represented by

$$\begin{aligned} \tilde{s}(t) &= \sqrt{\frac{E_b}{2N_f}} \sum_{m=-\infty}^{\infty} \sum_{i=0}^{N_f-1} g(t - mT_s - 2iT_d) + b_m g(t - mT_s - (2i+1)T_d) \\ &= \sqrt{\frac{E_b}{2N_f}} \sum_{m=-\infty}^{\infty} s_{b_m}(t - mT_s) \end{aligned} \tag{2.11}$$

where E_b is the average energy per bit, $b_m \in \{+1, -1\}$ is the data, $g(t)$ is the pulse shape with duration T_p resulting from the convolution of the transmit pulse $g_{tr}(t)$ with unit energy and the receiving filter matched to $g_{tr}(t)$, and $s_{b_m}(t) = \sum_{i=0}^{N_f-1} g(t -$

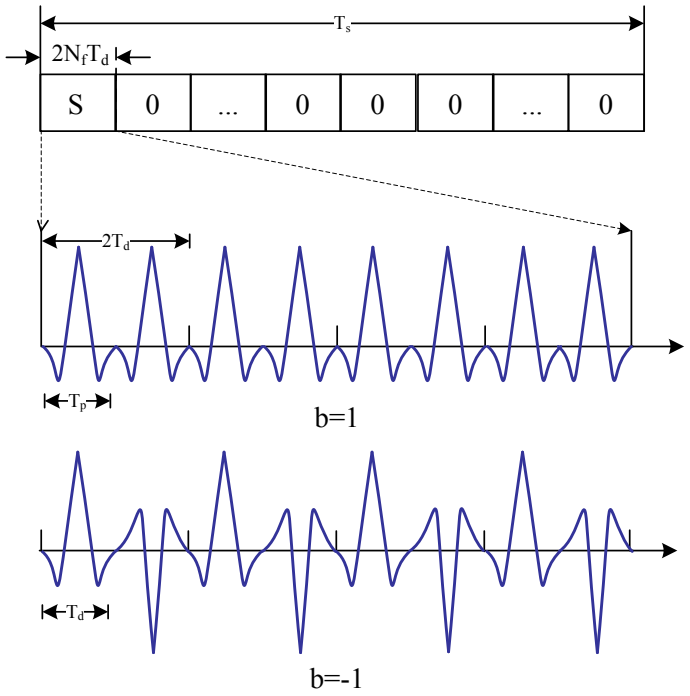

Figure 2.1: Pulse pattern of the proposed TRPC structure [1]

$2iT_d) + b_m \sum_{i=0}^{N_f-1} g(t-(2i+1)T_d)$. T_d is the small delay among all the pulses in the cluster, it can be as short as the pulse width T_p ($T_p \leq T_d \leq 10$ ns), e.g. $T_d = T_p$ as in Fig. 2.1.

Following IEEE 802.15.4a channel models [28] for UWB multipath environments, the channel can be expressed as

$$h(t) = \sum_{k=0}^{K-1} \alpha_k \delta(t - \tau_k) \tag{2.12}$$

where α_k and τ_k are the complex amplitude and delay of the k-th multipath. Then the m-th received signal can be written as

$$r(t) = \sqrt{\frac{E_b}{2N_f}} \sum_{k=0}^{K-1} \alpha_k s_{b_m}(t - \tau_k - mT_s) + n(t) = q_m(t - mT_s) + n(t) \tag{2.13}$$

where $q_m(t) = \sqrt{\frac{E_b}{2N_f}} \sum_{k=0}^{K-1} \alpha_k s_{b_m}(t-\tau_k)$, $n(t)$ is the complex additive white Gaussian noise (AWGN) passed through the receive filter $g_{tr}(-t)$, with autocorrelation function given by $R_n(\tau) = E[n^*(t)n(t+\tau)] = N_0 R_{tr}(\tau)$, N_0 is the power spectral density of the AWGN and $R_{tr}(\tau)$ is the autocorrelation function of $g_{tr}(-t)$.

The receiver performs auto-correlation on the received signal and its delayed version as illustrated in Fig. 2.2, where $r(t)$ represents the received signal.

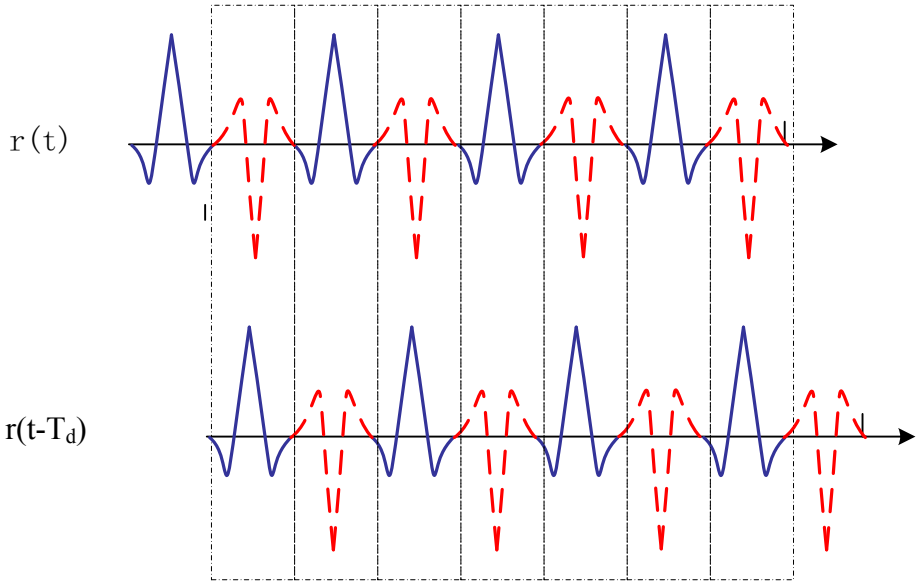

Figure 2.2: Energy collection in the TRPC receiver [1]

Then the decision variable (DV) for the m-th bit is obtained as

$$D = \int_{mT_s+T_1}^{mT_s+T_2} r(t) r^*(t - T_d) dt \tag{2.14}$$

where $[T_1, T_2]$ is the integration interval. The choices of $[T_1, T_2]$ should guarantee that the auto-correlation covers the significant channel portion plus a duration of $2(N_f - 1)T_d + T_p$ related to the pulse cluster width.

To capture sufficient channel energy for the detection, another important issue

lies in the selection of N_f. In implementation, N_f can not be too large; because in this case, the energy per pulse would be too low to combat the noise effect. In other words, a large N_f would lead to a longer pulse cluster and also a longer integration interval, which would introduce more noise to the autocorrelation receiver and impair the performance. In this thesis, N_f is chosen to be 4 following [1] for the simulation.

The receiver compares the real part of D ($\Re\{D\}$) with a threshold to make a decision on the data transmitted. The threshold can either be zero, that is the receiver makes a decision on "1" if $\Re\{D\} > 0$, and "0" if $\Re\{D\} < 0$; or the threshold can be an optimal threshold d in the maximum likelihood sense given by [1]

$$d = \frac{1}{2}\{m_D(+1) + m_D(-1)\} \tag{2.15}$$

where $m_D(+1)$ and $m_D(-1)$ denote the mean of $\Re\{D\}$ when $b_m = +1$ and $b_m = -1$, respectively. The adaptive threshold (2.15) results in much improved performance than the zero threshold and is adopted in this thesis.

2.2.2 TRPC System Performance

It was shown in [1] that $\Re\{D\}$ can be approximated as Gaussian distributed. Assuming that there is no inter-symbol interference (ISI), to derive the BER conditioned on one UWB channel $\mathbf{h}$, D can be splitted into the signal-signal component $\mathbf{D}_1$,

signal-and -noise product $\mathbf{D}_2$ and $\mathbf{D}_3$, and the noise-noise product $\mathbf{D}_4$ as

$$\begin{aligned} D &= \mathbf{D}_1 + \mathbf{D}_2 + \mathbf{D}_3 + \mathbf{D}_4 \\ \mathbf{D}_1 &= \int_{T_1}^{T_2} q(t)q^*(t-T_d)dt \\ \mathbf{D}_2 &= \int_{T_1}^{T_2} q(t)n^*(t-T_d)dt \\ \mathbf{D}_3 &= \int_{T_1}^{T_2} q^*(t-T_d)n(t)dt \\ \mathbf{D}_4 &= \int_{T_1}^{T_2} n(t)n^*(t-T_d)dt \end{aligned} \tag{2.16}$$

It can be easily shown that $E[\mathbf{D}_2 + \mathbf{D}_3] = 0$ and $E[\mathbf{D}_4] \approx 0$. Therefore, $m_D(b_m) = E[\Re\{D\}] \approx \Re\{\mathbf{D}_1\} = \int_{T_1}^{T_2} \Re\{q(t)q^*(t-T_d)\}dt$. The variance of $\Re\{D\}$ is the sum of the variances of $\sigma_{23}^2 = Var\left[\Re\{\mathbf{D}_2 + \mathbf{D}_3\}\right]$ and σ_4^2, that is $\sigma_D^2(b_m) = \sigma_{23}^2(b_m) + \sigma_4^2$. σ_{23}^2 and σ_2^4 can be derived as (2.17) and (2.18), respectively,

$$\begin{aligned} \sigma_{23}^2 &= Var[\Re\{\mathbf{D}_2\}] + Var[\Re\{\mathbf{D}_3\}] + 2E[\Re\{\mathbf{D}_2\}\Re\{\mathbf{D}_3\}] \\ Var[\Re\{\mathbf{D}_2\}] &= N_0 \int_{T_1}^{T_2}\int_{T_1}^{T_2} \Re\{q(t)q^*(t')\}R_{tr}(t'-t)dtdt' \\ Var[\Re\{\mathbf{D}_3\}] &= N_0 \int_{T_1}^{T_2}\int_{T_1}^{T_2} \Re\{q(t-T_d)q^*(t'-T_d)\}R_{tr}(t'-t)dtdt' \\ E[\Re\{\mathbf{D}_2\}\Re\{\mathbf{D}_3\}] &= N_0 \int_{T_1}^{T_2}\int_{T_1}^{T_2} \Re\{q(t)q^*(t'-T_d)\}R_{tr}(t'-t+T_d)dtdt' \end{aligned} \tag{2.17}$$

$$\sigma_4^2 = Var[\Re\{\mathbf{D}_4\}] = \frac{N_0^2}{2}\int_{-\frac{T_i}{\sqrt{2}}}^{\frac{T_i}{\sqrt{2}}} (\sqrt{2}T_i - 2|y|))R_{tr}^2(\sqrt{2}y)dy, \tag{2.18}$$

where $T_i = T_2 - T_1$.

Because the "+1" pulse cluster is not the simple opposite of "-1", the error probability of "+1" pulse cluster is not necessarily identical to that of the "-1" pulse cluster. Thus the probability of error conditioned on channel realization $\mathbf{h}$ using the

hard decision is given by [1]

$$\begin{aligned} P(e|\mathbf{h}) &= P(e|\mathbf{h}, b_m = 1)P(b_m = 1) + P(e|\mathbf{h}, b_m = -1)P(b_m = -1) \\ &= \frac{1}{2}Q\left(\frac{-m_D(-1)}{\sqrt{\sigma_{23}^2(-1) + \sigma_4^2}}\right) + \frac{1}{2}Q\left(\frac{m_D(1)}{\sqrt{\sigma_{23}^2(1) + \sigma_4^2}}\right). \end{aligned} \tag{2.19}$$

And the BER using adaptive threshold is given by [1]

$$P(e|\mathbf{h}) = Q\left(\frac{-m_D(-1) + m_D(+1)}{\sqrt{\sigma_D^2(-1) + \sigma_D^2(+1)}}\right) \tag{2.20}$$

where σ_D^2 represents the variance of $\Re\{D\}$.

2.3 Cooperative Network Structure

In a two-way-relay system, there is no direct link between the two users, and information is exchanged with the help of the relay. Usually, two phases are used in the protocol of a two-way-relay system, namely the multiple-access (MA) phase and the broadcast (BC) phase. In the MA phase, information is sent from the source nodes to the relay. While in the BC phase, the relay broadcasts the processed information. Both phases are carried out either over a time division duplex (TDD) mode or a frequency division duplex (FDD) mode [31].

In this thesis, a bi-directional network with two relays between two users is investigated, as shown in Fig. 2.3. There are four independent channels $\mathbf{h}_1$, $\mathbf{h}_2$, $\mathbf{h}_3$ and $\mathbf{h}_4$ between the source (S_1, S_2) and relay (R_1, R_2) nodes, each of the nodes works in a half-duplex mode; and no direct link exists between the two sources. Hence information is exchanged with the help of the relays. Message is transmitted through channels $\mathbf{h}_1$, $\mathbf{h}_2$ and R_1, and/or through $\mathbf{h}_3$, $\mathbf{h}_4$ and R_2.

As it has been mentioned above, a UWB system is limited in its transmit power,

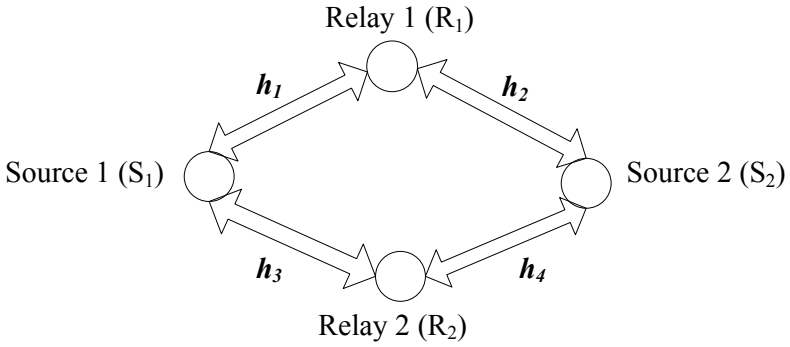

Figure 2.3: Cooperative network structure

as specified by the regulatory spectrum mask. Thus the maximum transmit power is assumed to be the same at all transmitters throughout this thesis. On the other hand, the TDD mode is adopted in this thesis, and each frame of the communication is separated into four equal time slots, which means that the multiple-access phase contains the first two time slots, and time slots 3 and 4 make up the broadcast phase in the communication, as shown in Fig. 2.4.

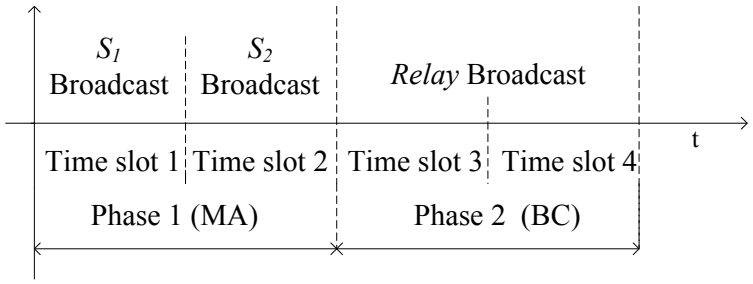

Figure 2.4: Preliminary cooperation mode structure

In the MA phase employing TDMA, the two source nodes broadcast their information successively in two time slots. Both relays receive and decode the broadcast signals from S_1 in the first time slot and from S_2 in the second time slot, hence there is no interference among the users. Then each relay performs physical layer network coding by "xor" the decoded bits from the two sources, which will save one time slot

for the relay to forward the information to the two sources. And in the BC phase, relays broadcast the PNC coded bits according to various cooperative strategies which will be presented in Chapter 3 and 4.

Chapter 3

Cooperative Strategies for UWB TRPC Networks

In this Chapter, five cooperative relay strategies for the UWB TRPC networks are proposed. The plain Relay Combining (RC) strategy without any selection is investigated as a reference first, followed by four relay selection cooperative strategies, which are based on two newly defined channel quality indicators.

3.1 Relay Combining (RC)

3.1.1 RC Cooperative Structure

The cooperative structure for the RC strategy is shown in Fig. 3.1. In the MA phase, R_1 and R_2 receive and decode the information from S_1 (in time slot 1) and S_2 (in time slot 2), and perform the "xor" operation to the two decoded bits respectively, hence the PNC bits b_{r_1} and b_{r_2} are obtained at R_1 and R_2. In the BC phase, R_1 broadcasts b_{r_1} back to both sources in time slot 3 and R_2 broadcasts b_{r_2} in time slot 4. Due to detection errors in the first phase, R_1 and R_2 may have different PNC bits to send

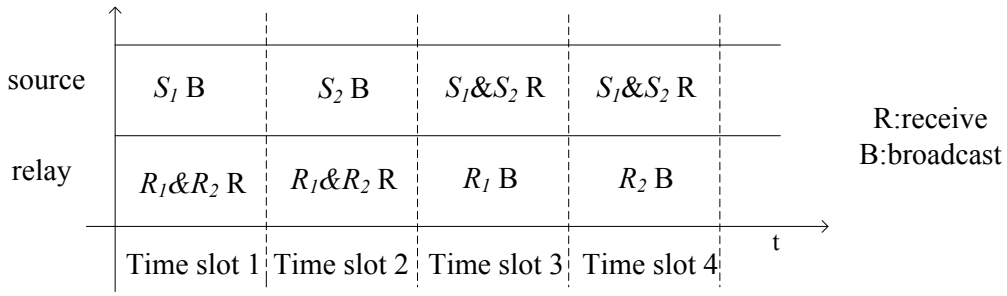

Figure 3.1: Cooperative structure for the RC strategy

(that is, $b_{r_1} \neq b_{r_2}$), leading to the problem of error propagation.

In the BC phase, each source node receives two decision variables from both relays separately, and then adds them up to make the decision. For example, S_1 will obtain D_1 via channel $\mathbf{h}_1$ and D_3 via channel $\mathbf{h}_3$ in time slots 3 and 4 successively, and then the node adds them linearly (D_1+D_3) to get the new DV, and makes a decision according to the threshold (d_1+d_3). Similar operation is taken at S_2. To extract the information from the other source, "xor" operation is done between the received bit and the local information bit at the source.

In the RC scenario, no selection of relays is needed, thus a relative simple structure will work for the receiver. As well, the relays work independently in different time slots, so communications between the relays are not necessary.

3.1.2 RC System Performance Analysis

In this subsection, numerical analysis is given towards the BER performance of the RC strategy. First, denote P_i (i = 1, 2, 3, 4) as the error probability of one hop communication conditioned on the channel realization $\mathbf{h}_i$, which is given by (2.20).

Then the bit error probability at R_j after PNC, $P_{r_j}(\mathbf{h}_{2j-1}, \mathbf{h}_{2j})$ $(j = 1, 2)$ becomes

$$\begin{aligned} P_{r_j}(e|\mathbf{h}_{2j-1}, \mathbf{h}_{2j}) &= 1 - P_{2j-1}P_{2j} - (1 - P_{2j-1})(1 - P_{2j}) \\ &= P_{2j-1} + P_{2j} - 2P_{2j-1}P_{2j}. \end{aligned} \tag{3.1}$$

Furthermore, the BER at the Source node i (i=1, 2), $P_e(s_i)$, is given by

$$\begin{aligned} P_e(s_i) &= (1 - P(\hat{b}_{s_i} \neq b_{r_1}|b_{r_1} = b_{r_2}))P_{r_1}P_{r_2} + P(\hat{b}_{s_i} = b_{r_2}|b_{r_1} \neq b_{r_2})(1 - P_{r_1})P_{r_2} \\ &+ P(\hat{b}_{s_i} = b_{r_1}|b_{r_1} \neq b_{r_2})P_{r_1}(1 - P_{r_2}) + P(\hat{b}_{s_i} \neq b_{r_1}|b_{r_1} = b_{r_2})(1 - P_{r_1})(1 - P_{r_2}) \end{aligned} \tag{3.2}$$

where $b_{r_j}(j = 1, 2)$ represents the bit sent from R_j, and $\hat{b}_{s_i}$ stands for the decoded bit at S_i after combining the DVs from the two relays. The conditional probability $P(\hat{b}_{s_i} = b_{r_2}|b_{r_1} \neq b_{r_2})$, is equal to $1 - P(\hat{b}_{s_i} = b_{r_1}|b_{r_1} \neq b_{r_2})$, and shows the probability that the two relays have opposite PNC bits to broadcast, while the decoded bit at S_i is the same with that from R_2. Moreover, $P(\hat{b}_{s_1} \neq b_{r_1}|b_{r_1} = b_{r_2})$, $P(\hat{b}_{s_1} = b_{r_1}|b_{r_1} \neq b_{r_2})$ and $P(\hat{b}_{s_2} \neq b_{r_1}|b_{r_1} = b_{r_2})$, $P(\hat{b}_{s_2} = b_{r_1}|b_{r_1} \neq b_{r_2})$ can be derived as (3.3) and (3.4), respectively.

$$\begin{aligned} P(\hat{b}_{s_1} \neq b_{r_1}|b_{r_1} = b_{r_2}) &= Q\left(\frac{-(m_1(-1) + m_3(-1)) + (m_1(1) + m_3(1))}{\sqrt{\sigma_1^2(-1) + \sigma_3^2(-1) + \sigma_1^2(1) + \sigma_3^2(1)}}\right) \\ P(\hat{b}_{s_1} = b_{r_1}|b_{r_1} \neq b_{r_2}) &= Q\left(\frac{-(m_1(1) + m_3(-1)) + (m_1(-1) + m_3(1))}{\sqrt{\sigma_1^2(1) + \sigma_3^2(-1) + \sigma_1^2(-1) + \sigma_3^2(1))}}\right) \end{aligned} \tag{3.3}$$

$$\begin{aligned} P(\hat{b}_{s_2} \neq b_{r_1}|b_{r_1} = b_{r_2}) &= Q\left(\frac{-(m_2(-1) + m_4(-1)) + (m_2(1) + m_4(1))}{\sqrt{\sigma_2^2(-1) + \sigma_4^2(-1) + \sigma_2^2(1) + \sigma_4^2(1)}}\right) \\ P(\hat{b}_{s_2} = b_{r_1}|b_{r_1} \neq b_{r_2}) &= Q\left(\frac{-(m_2(1) + m_4(-1)) + (m_2(-1) + m_4(1))}{\sqrt{\sigma_2^2(1) + \sigma_4^2(-1) + \sigma_2^2(-1) + \sigma_4^2(1))}}\right) \end{aligned} \tag{3.4}$$

Finally, because the two users exchange same amount of information, the performance of the whole system can be derived from the average of the two source nodes, that is

$$P_{RC}(e) = \frac{1}{2}\left(P_e(s_1) + P_e(s_2)\right) \tag{3.5}$$

3.1.3 RC Simulation Results

To demonstrate that the RC strategy with adaptive threshold will outperform the case with the zero threshold, as well as to validate the reliability of the theoretical results, the simulation results following the RC strategy are shown in Fig. 3.2.

The experiment is taken under the IEEE 802.15.4a CM1 channels, which stands for the strong line-of-sight (LOS) environment. The transmit pulse shape and the receiver filter ($g_{tr}(-t)$ in Section 2.2.1) adopt the root raised cosine (RRC) pulse with roll-off factor $\beta = 0.25$. The zero-to-zero main lobe width of the RRC pulse is $T_p = 2.02$ ns, and the pulse cluster is composed of 8 contiguous pulses, i.e., $N_f = 4$. The pulse cluster length is then $T_u = 16.16$ ns. Low bit rate of 1 Mbps under CM1 channels are studied, and hence the system is ISI free. The sampling rate of the receiver analog-to-digital (A/D) device is equal to the symbol rate. The integration interval related parameters T_1 and T_2 are determined as the beginning and end paths of the channel, with magnitude larger than a fraction of the channel maximum magnitude. In other words, any multipath components before T_1 and after T_2 are smaller than $s \cdot \max(|\alpha_k|_{k=0}^{K-1})$, where s (= 0.3 in the simulation) is the scale factor and α_k is the k-th path gain [30].

From Fig. 3.2, it is seen that the analytical results agree with simulation curves, validating the theoretical analysis. Moreover, the numerical results demonstrate that by using the adaptive threshold, substantial performance gain is achieved over the zero threshold in the two-way-relay network. For example, at BER around $3 * 10^{-4}$,

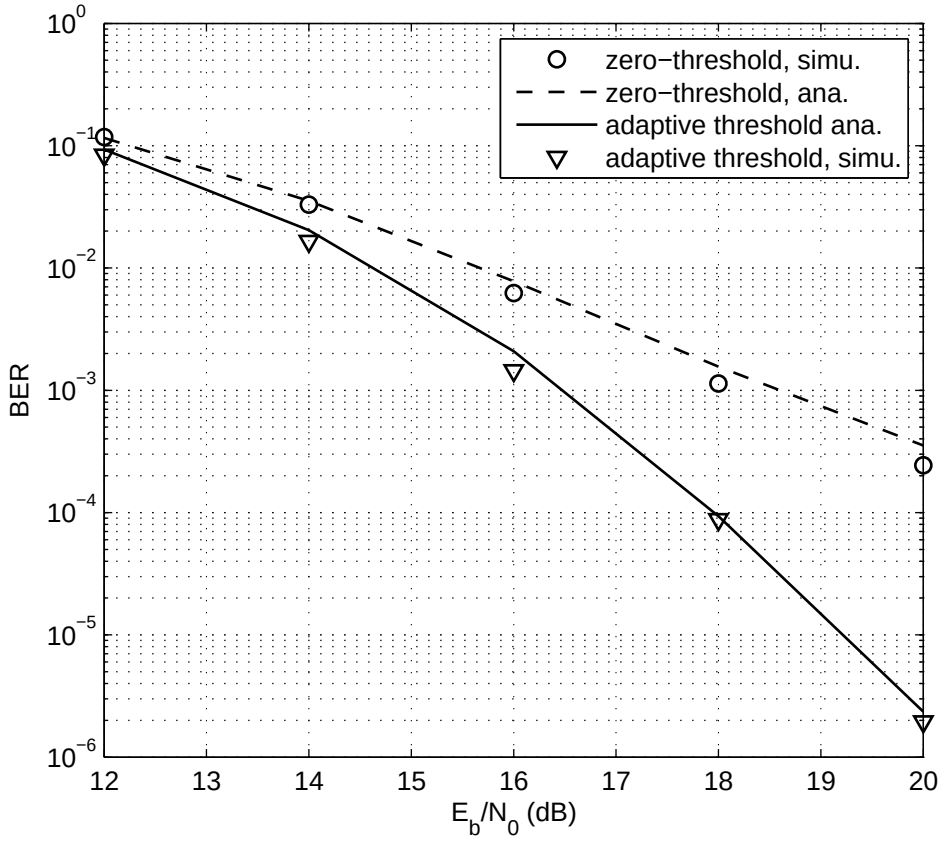

Figure 3.2: Simulation results for RC cooperative strategy under CM1 channel environment

2.6 dB gain is realized in CM1 channels.

3.2 Weighted Relay Combining (WRC)

In the RC strategy above, the system performance will degrade if the two relays broadcast different PNC bits due to the error(s) in the first phase S-R links. One possible remedy is to weight the transmit power at the relay whose associated channels are in poor condition. Since a TRPC autocorrelation receiver does not estimate the UWB channel for low complexity, we want to find a quantity that can reflect the quality of a channel without requiring the full knowledge of the channel.

In the following subsections, a novel Decision Variable based channel quality indicator (M) is proposed first, and the Weight Relay Combining (WRC) strategy is further introduced based on the indicator.

3.2.1 Normalized Channel Quality Indicator

The normalized channel quality indicator M_i is defined here for channel $\mathbf{h}_i$, as

$$M_i = \frac{|D_i - d_i|}{E_i} \tag{3.6}$$

where D_i is the decision variable (DV) conditioned on channel $\mathbf{h}_i$ and the information bit b_m, as given by (2.14). d_i stands for the adaptive threshold, which is defined in (2.15). And E_i can be calculated as

$$E_i = \frac{1}{2}\{m_i(+1) - m_i(-1)\} \tag{3.7}$$

where $m_i(b_m)$ represents $m_D(b_m)$ for the channel realization $\mathbf{h}_i$.

M_i is the distance of the DV to the decision threshold, normalized by the distance

between the noiseless DV and the decision threshold. It can directly reflect the reliability of the detection; the larger the M_i, the less likely that a decision error will be made. The values d_i and E_i can be estimated for the particular channel through training sequences. Since UWB applications mainly focus on indoor environments, the time variation of the channels are insignificant and hence the training does not need to be done frequently.

3.2.2 WRC Cooperative Strategy

Based on the channel quality indicator M, an outage (OT_i) for a TRPC UWB channel is further defined, as the event that M_i is less than a pre-determined threshold ϱ ($\varrho < 1$). That is

$$OT_i = \begin{cases} 1, & M_i < \varrho \\ 0, & M_i \geq \varrho. \end{cases} \tag{3.8}$$

As the value of M can reflect the channel condition, thus when an outage happens, the decoded bit at relays experiences a higher chance being in error in the MA phase. The idea of the WRC strategy is to weigh the transmit power at relays based on the channel outage. That is, the higher probability a link has to experience a bad channel condition in the MA phase, the less responsibility the corresponding relay will assume to broadcast the information in the BC phase. The cooperation mode for the WRC strategy is the same with that for the RC case shown in Fig. 3.1.

We assume that the transmit power is limited by ϵ at all transmitters, and define M_i' as

$$M_i' = \begin{cases} M_i, & OT_i = 1 \\ 1\ , & OT_i = 0, \end{cases} \tag{3.9}$$

where M_i' is less than 1, as a result of $\varrho < 1$.

Then in the WRC strategy, the transmit signal amplitude at R_j $(j = 1, 2)$ is scaled by β_j according to the relay detection, which should be smaller than or equal to 1, defined by

$$\beta_j = \sqrt{M'_{2j-1} \times M'_{2j}} \tag{3.10}$$

Because of the scaling at the relays, the adaptive threshold d_i at the receiver in the BC phase for channel $\mathbf{h}_i$ changes to

$$d'_i = \beta_j^2 \times d_i, \tag{3.11}$$

where $i = 2j$ or $i = 2j - 1$. In the BC phase, at the receiver side (e.g. S_1), D_1 from $\mathbf{h}_1$ and D_3 from $\mathbf{h}_3$ are added linearly to make the decision according to the threshold $(d'_1 + d'_3)$.

Recall the network in Fig. 2.3, to analyze the system BER performance of the WRC strategy compared with RC, hop $\mathbf{h}_2$ can be assumed to be in an outage without loss of generality, and hence $P_2 \gg P_1, P_3$ and P_4. As ϱ is usually selected to be much smaller than 1 (e.g., 0.2 in this thesis), the DV at S_1 from channel $\mathbf{h}_1$, D_1 (after weighting at relay) becomes negligible compared with D_3, thus the error rate at S_1, $P_e^{WRC}(s_1)$ can be briefly estimated by the unimpaired link through $\mathbf{h}_4$, R_2 and $\mathbf{h}_3$, that is

$$\begin{aligned} P_e^{WRC}(s_1) \approx P_{S_1}^{l_2} &= 1 - [P_{r_2}P_3 + (1 - P_{r_2})(1 - P_3)] \\ &= P_{r_2} + P_3 - 2P_{r_2}P_3 \end{aligned} \tag{3.12}$$

where $P_{S_1}^{l_2}$ is the BER at S_1 via the R_2 link only, and P_{r_2} can be derived from (3.1).

On the other hand, the BER at S_1 from the RC strategy $P_e^{RC}(s_1)$ can be derived

as

$$\begin{aligned} P_e^{RC}(s_1) &= P_{S_1}^{l_1} P_{S_1}^{l_2} + P_{S_1}^{l_2}(1 - P_{S_1}^{l_1}) P(D_3 > D_1) + (1 - P_{S_1}^{l_2}) P_{S_1}^{l_1} P(D_3 < D_1) \\ &= P_{S_1}^{l_1} P_{S_1}^{l_2} + P_{S_1}^{l_2}(1 - P_{S_1}^{l_1}) \left(1 - P(D_1 > D_3)\right) + (1 - P_{S_1}^{l_2}) P_{S_1}^{l_1} P(D_3 < D_1) \\ &= P_{S_1}^{l_2} + (P_{S_1}^{l_1} - P_{S_1}^{l_2}) P(D_1 > D_3), \end{aligned} \tag{3.13}$$

where $P(D_3 > D_1)$ stands for the probability that the DV from channel $\mathbf{h}_3$ (D_3) is larger than that from $\mathbf{h}_1$ (D_1). It is obvious that $P_{S_1}^{l_1}$ is larger than $P_{S_1}^{l_2}$ as the assumption that $\mathbf{h}_2$ is in an outage, and $P(D_1 > D_3) \geq 0$; thus $P_e^{RC}(s_1) > P_e^{WRC}(s_1)$, and similar analysis can be derived at S_2, which means the WRC strategy has a lower BER than the RC case.

In conclusion, since the relay with relatively poor channel conditions are scaled down in the transmit power following the WRC strategy, its error-prone DV has smaller effect on the final DV at the receiver, and hence improving the system performance compared with the RC case.

3.3 Outage Based Relay Selection (ORS)

In either of the RC or WRC strategy, both relays will participate in the cooperation without any selection. In this section, another relay cooperative strategy is introduced, namely the Outage based Relay Selection (ORS) strategy, where either one selected relay or both relays participate in the cooperation. The cooperation mode of the ORS strategy is shown in Fig. 3.3.

In the MA phase, there are four independent channels S_i-R_j $(i, j = 1, 2)$. Three cases may happen according to the relay detection as:

A . If no channel is detected to be in an outage, both relays will forward the PNC

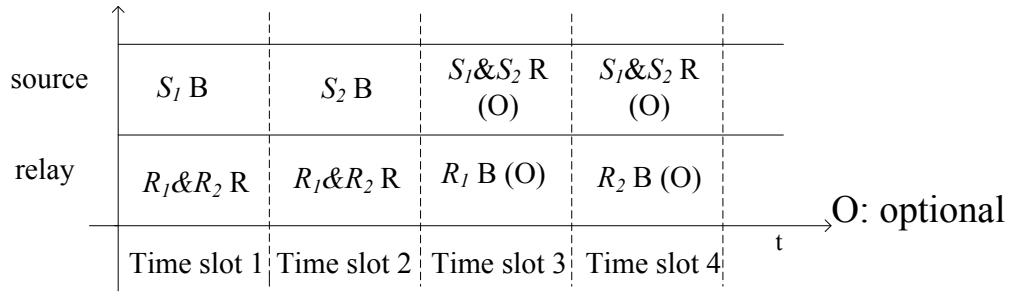

Figure 3.3: Cooperative structure for the ORS strategy

data from S_1 and S_2, the same as the RC strategy.

B . If the channel(s) in outage is (are) associated with one relay only, the relay with unimpaired channels will be selected to broadcast in the BC phase.

C . Otherwise, relay selection is determined by comparing $M_1 \times M_2$ and $M_3 \times M_4$. R_1 will be chosen if $M_1 \times M_2 \geq M_3 \times M_4$; otherwise, R_2 will be selected.

The flowchart of the ORS strategy is presented in Fig. 3.4.

Relay weighting is needed in the WRC strategy, and relay selection is used in the ORS strategy, none of which is needed in the RC case. In the WRC scheme, relays work independently; whereas, talks need to be established between the relays in the ORS scenario, whenever relay selection needs to be made as mentioned in case **B** and **C** above.

3.4 Maximum Product Relay Selection (MP-RS)

In the three cooperative strategies above, both relays have opportunities to participate in the cooperation. In this and next subsections, two relay selection schemes are introduced. The idea is to select one relay with better channel conditions first and

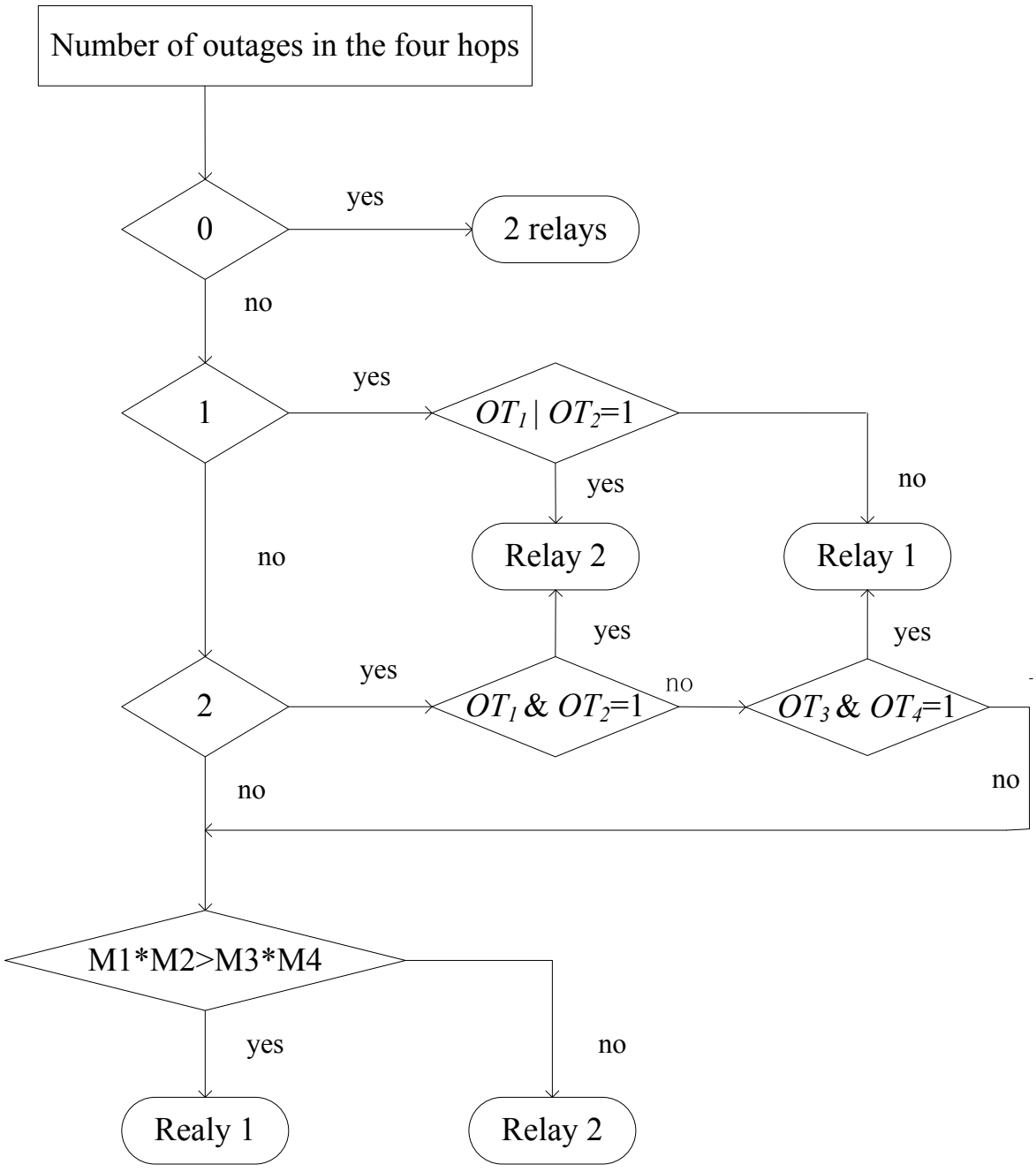

Figure 3.4: Flow chart for the ORS cooperative strategy

then let the chosen relay broadcast twice in the BC phase. The cooperation mode of the MP-RS strategy is shown in Fig. 3.5. The chosen relay R_c will forward the same

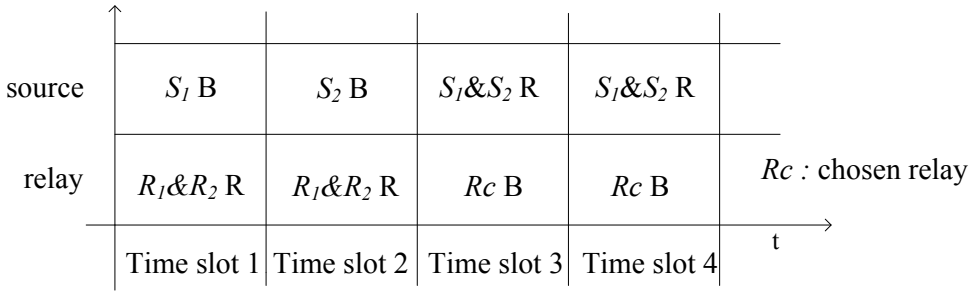

Figure 3.5: Cooperative structure for the MP-RS strategy

information in time slot 3 and 4 separately, in order to keep a consistent data rate with the other three cooperative strategies, and hence a denoising gain is obtained. R_c may change from bit to bit depending on the Maximum Product selection criterion.

The MP-RS strategy selects the cooperative relay based on the product of M_i defined in (3.6). That is, when $M_1 \times M_2 \geq M_3 \times M_4$, R_1 is chosen; otherwise, R_2 broadcasts in the second phase.

The implementation of such relay selections can be carried out similar to the opportunistic relaying proposed in [32] by using a timer in each relay, and the timer is set according to the value of $1/(M_{2j-1}M_{2j}), j = 1, 2$. The relay with timer expired first gets to send and the other relay hearing the transmission will not send.

Since the chosen relay sends twice the PNC bit, the receiver adds the two decision variables linearly and makes decisions accordingly. As a result, the signal-to-noise ratio is doubled, and the BER for the second phase transmission from one relay to one source becomes (in contrast to Eq. (2.20))

$$\hat{P}_i(e|\mathbf{h_i}) = Q\left(\frac{-\sqrt{2}m_i(-1) + \sqrt{2}m_i(1)}{\sqrt{\sigma_i^2(-1) + \sigma_i^2(1)}}\right) \tag{3.14}$$

where $\sigma_i^2(b_m)$ $(i = 1, 2, 3, 4)$ stands for $\sigma_D^2(b_m)$ for the channel realization $\mathbf{h}_i$.

3.5 Minimax Relay Selection (MinMax-RS)

In this section, a Minimax relay selection (MinMax-RS) strategy is introduced. The cooperation mode of the MinMax-RS strategy is the same as that of the MP-RS scheme shown in Fig. 3.5. However, they have different criterions towards the relay selection.

3.5.1 Channel Quality Indicator M based MinMax-RS

In the MinMax-RS strategy, denote $Z^1 = \min(M_1, M_2)$ and $Z^2 = \min(M_3, M_4)$, then R_1 will be chosen when $Z^1 \geq Z^2$; otherwise, R_2 is selected for the cooperation in the BC phase. Similar to the MP-RS strategy, the timer in each relay can be set according to the value of $1/\min(M_{2j-1}, M_{2j}), j = 1, 2$.

The BER performance of the MinMax-RS for bi-directional transmission can be derived as

$$P_{MinMax-RS} = \sum_{m=0}^{1}\sum_{n=0}^{1} P(s_1 = m, s_2 = n) \times [BER(\text{link1}|Z^1 \geq Z^2)P(Z^1 \geq Z^2|s_1 = m, s_2 = n) + BER(\text{link2}|Z^1 < Z^2)P(Z^1 < Z^2|s_1 = m, s_2 = n)], \quad (3.15)$$

where s_1, s_2 are the information bits at S_1 and S_2 with equal priori probabilities $(P(s_j = 0) = P(s_j = 1) = \frac{1}{2}, j = 1, 2)$, respectively. $BER(\text{link1}|Z^1 \geq Z^2)$ and $BER(\text{link2}|Z^1 < Z^2)$ represent the BERs of the bi-directional end-to-end transmission conditioned on R_1 or R_2 is being selected.

Recall that the decision variables D_i $(i = 1, \ldots, 4)$ can be approximated by Gaussian Random Variables (RVs). That is, $D_i \sim \mathcal{N}(a_i, b_i^2)$, where $a_i \in \{m_i(+1), m_i(-1)\}$

and $b_i \in \{\sigma_i(+1), \sigma_i(-1)\}$. Thus the cumulative distribution functions (CDF) and the probability distribution functions (PDF) of M_i can be derived as

$$\begin{aligned} F_{M_i}(r) &= \mathbf{P}(M_i \leq r) = \mathbf{P}\left(-r \leq \frac{D_i - d_i}{E_i} \leq r\right) \\ &= \mathbf{P}(d_i - rE_i \leq D_i \leq d_i + rE_i) = \frac{1}{\sqrt{2\pi}b_i} \int_{-E_i r + d_i}^{E_i r + d_i} e^{-\frac{(x-a_i)^2}{2b_i^2}} dx \\ &= Q\left(\frac{-E_i r - a_i + d_i}{b_i}\right) - Q\left(\frac{E_i r - a_i + d_i}{b_i}\right). \end{aligned} \tag{3.16}$$

$$f_{M_i}(r) = \frac{dF_{M_i}(r)}{dr} = \frac{E_i}{\sqrt{2\pi}b_i}\left(e^{-\frac{(E_i r - a_i + d_i)^2}{2b_i^2}} + e^{-\frac{(-E_i r - a_i + d_i)^2}{2b_i^2}}\right). \tag{3.17}$$

According to the definition of Z^1, its CDF ($F_{Z^1}(r)$) can be obtained by

$$\begin{aligned} F_{Z^1}(r) &= P(Z^1 \leq r) = 1 - P(Z^1 > r) \\ &= 1 - P(M_1 > r, M_2 > r) = 1 - P(M_1 > r)P(M_2 > r) \\ &= 1 - [1 - F_{M_1}(r)][1 - F_{M_2}(r)] \\ &= F_{M_1}(r) + F_{M_2}(r) - F_{M_1}(r)F_{M_2}(r). \end{aligned} \tag{3.18}$$

Hence the PDF of Z^1 ($f_{Z^1}(r)$) can be derived as

$$f_{Z^1}(r) = f_{M_1}(r) + f_{M_2}(r) - F_{M_1}(r)f_{M_2}(r) - F_{M_2}(r)f_{M_1}(r). \tag{3.19}$$

Similarly, we can get the PDF of Z^2 ($f_{Z^2}(r)$) as

$$f_{Z^2}(r) = f_{M_3}(r) + f_{M_4}(r) - F_{M_3}(r)f_{M_4}(r) - F_{M_4}(r)f_{M_3}(r). \tag{3.20}$$

$P(Z^1 \geq Z^2 | s_1, s_2)$ in (3.15) represents the probability Z^1 is equal to or larger than Z^2,

conditioned on s_1 and s_2. $P(Z^1 \geq Z^2|s_1, s_2)$ and $P(Z^1 < Z^2|s_1, s_2)$ can be derived as

$$\begin{aligned} P(Z^1 \geq Z^2|s_1, s_2) &= \int_0^{\infty} \int_0^{\gamma_1} f_{Z^1}(\gamma_1) f_{Z^2}(\gamma_2)\ d\gamma_2\ d\gamma_1 \\ &= \int_0^{\infty} f_{Z^1}(\gamma_1)\left[F_{M_3}(\gamma_1) + F_{M_4}(\gamma_1) - F_{M_3}(\gamma_1)F_{M_4}(\gamma_1)\right] d\gamma_1 \\ P(Z^1 < Z^2|s_1, s_2) &= \int_0^{\infty} \int_0^{\gamma_2} f_{Z^1}(\gamma_1) f_{Z^2}(\gamma_2)\ d\gamma_1\ d\gamma_2 \\ &= \int_0^{\infty} f_{Z^2}(\gamma_2)\ \left[F_{M_1}(\gamma_2) + F_{M_2}(\gamma_2) - F_{M_1}(\gamma_2)F_{M_2}(\gamma_2)\right] d\gamma_2. \end{aligned} \tag{3.21}$$

The $BER(\text{link1}|Z^1 \geq Z^2)$ and $BER(\text{link2}|Z^1 < Z^2)$ in (3.15) can be written as

$$\begin{aligned} BER(\text{link1}|Z^1 \geq Z^2) &= \frac{1}{2}(\hat{P}_1 + P'_{r_1} - 2\hat{P}_1 P'_{r_1} + \hat{P}_2 + P'_{r_1} - 2\hat{P}_2 P'_{r_1}) \\ BER(\text{link2}|Z^1 < Z^2) &= \frac{1}{2}(\hat{P}_3 + P'_{r_2} - 2\hat{P}_3 P'_{r_2} + \hat{P}_4 + P'_{r_2} - 2\hat{P}_4 P'_{r_2}). \end{aligned} \tag{3.22}$$

where $\hat{P}_i$ is the error probability of the relay to source transmission (twice) in the BC phase given by Eq. (3.14), and P'_{r_j} is the error probability of the PNC coded bit at R_j, conditioned on R_j being selected.

As a result of the relay selection, the reliability of communication in the MA phase increases. Thus the distribution of D_i for the selected channel $\mathbf{h}_i$ in the MA phase changes to D'_i, leading to a different error probability (P'_i) from source to relay.

Here D'_1 is taken as an example to formulate P'_1, where P'_1 is the new BER conditioned on link 1 being selected, and then P'_{r_1} can be calculated from P'_1 and P'_2 as (3.1). D_2-D_4 can be derived in a similar manner.

The CDF of the noise term n_1' in D_1' is given by

$$\begin{aligned} F_{n_1'}(x) = P(n_1' \leq x) = & \int_{-\infty}^{x} f_{n_1}(n_1) \int_{M_1(n_1) \geq M_2(n_2)} f_{n_2}(n_2) \int_{Z^1(n_2) \geq Z^2(\gamma_2)} d\gamma_2 \; dn_2 \; dn_1 \\ + & \int_{-\infty}^{x} f_{n_1}(n_1) \int_{M_1(n_1) < M_2(n_2)} f_{n_2}(n_2) \; dn_2 \int_{Z^1(n_1) \geq Z^2(\gamma_2)} d\gamma_2 \; dn_1. \end{aligned} \tag{3.23}$$

Then its corresponding PDF can be derived as

$$\begin{aligned} f_{n_1'}(x) = \frac{d \; F_{n_1'}(x)}{d \; x} = & \quad f_{n_1}(x) \Big[F_{n_2}\left(A_1(x)\right) + 1 - F_{n_2}\left(A_2(x)\right) \Big] \int_0^{B(x)} f_{Z^2}(\gamma_2) d\gamma_2 \\ + & \quad f_{n_1}(x) \int_{A_1(x)}^{A_2(x)} \int_0^{C(n_2)} f_{n_2}(n_2) f_{Z^2}(\gamma_2) \; d\gamma_2 \; dn_2 \end{aligned} \tag{3.24}$$

where $f_{n_1}(n_1)$ and $f_{n_2}(n_2)$ are the PDFs of the noise terms in D_1 and D_2 with no relay selection, respectively, and they are zero mean Gaussian with variance $\sigma_1^2(s_1)$ and $\sigma_2^2(s_2)$. $F_{n_1}(n_1)$ and $F_{n_2}(n_2)$ are their corresponding CDFs. Moreover,

1. $s_1 = s_2 = 1$

$$\begin{cases} A_1\left(x\right) & = -\frac{E_2}{E_1} \left|E_1 + x\right| - E_2 \\ A_2\left(x\right) & = \frac{E_2}{E_1} \left|E_1 + x\right| - E_2 \\ B\left(x\right) & = \frac{|E_1 + x|}{E_1} \\ C\left(n_2\right) & = \frac{|E_2 + n_2|}{E_2} \end{cases}$$

$$P_1' = \int_{-\infty}^{-E_1} \frac{f_{n_1'}(n_1')}{P(Z^1 \geq Z^2 | s_1 = s_2 = 1)} dn_1' \tag{3.25}$$

2. $s_1 = s_2 = 0$

$$\begin{cases} A_1(x) & = -\frac{E_2}{E_1}|-E_1+x| + E_2 \\ A_2(x) & = \frac{E_2}{E_1}|-E_1+x| + E_2 \\ B(x) & = \frac{|-E_1+x|}{E_1} \\ C(n_2) & = \frac{|-E_2+n_2|}{E_2} \end{cases}$$

$$P_1' = \int_{E_1}^{\infty} \frac{f_{n_1'}(n_1')}{P(Z^1 \geq Z^2 | s_1 = s_2 = 0)} dn_1' \tag{3.26}$$

3. $s_1 = 1, s_2 = 0$

$$\begin{cases} A_1(x) & = -\frac{E_2}{E_1}|E_1+x| + E_2 \\ A_2(x) & = \frac{E_2}{E_1}|E_1+x| + E_2 \\ B(x) & = \frac{|E_1+x|}{E_1} \\ C(n_2) & = \frac{|-E_2+n_2|}{E_2} \end{cases}$$

$$P_1' = \int_{-\infty}^{-E_1} \frac{f_{n_1'}(n_1')}{P(Z^1 \geq Z^2 | s_1 = 1, s_2 = 0)} dn_1' \tag{3.27}$$

4. $s_1 = 0, s_2 = 1$

$$\begin{cases} A_1(x) & = -\frac{E_2}{E_1}|-E_1+x| - E_2 \\ A_2(x) & = \frac{E_2}{E_1}|-E_1+x| - E_2 \\ B(x) & = \frac{|-E_1+x|}{E_1} \\ C(n_2) & = \frac{|E_2+n_2|}{E_2} \end{cases}$$

$$P_1' = \int_{E_1}^{\infty} \frac{f_{n_1'}(n_1')}{P(Z^1 \geq Z^2 | s_1 = 0, s_2 = 1)} dn_1' \tag{3.28}$$

In both of the MP-RS and MinMax-RS strategies, selections should be made between the relays; and the source nodes require the results of selection in order to make decisions accordingly. However, in the other three strategies, the two relays work in their specified time slots regardless of the relay selection, thus there is less overhead in the BC phase. Simulations in Section 3.6 show that the MP-RS and MinMax-RS strategies gain a better performance with a slightly higher overhead cost than the RC, WRC and ORS ones.

3.5.2 Channel Quality Indicator LLR based MinMax-RS Strategy

In this section, another channel quality indicator LLR_i based on the Log Likelihood Ratio (LLR) for channel $\mathbf{h}_i$ is introduced, which is defined as

$$\begin{aligned} LLR_i &= \log \left[\frac{\frac{1}{\sqrt{2\pi}\sigma_i(\hat{b}_m)} e^{-\frac{(D_i - m_i(\hat{b}_m))^2}{2\sigma_i^2(\hat{b}_m)}}}{\frac{1}{\sqrt{2\pi}\sigma_i(\tilde{\hat{b}}_m)} e^{-\frac{\left(D_i - m_i(\tilde{\hat{b}}_m)\right)^2}{2\sigma_i^2(\tilde{\hat{b}}_m)}}} \right] \\ &= \log \left[\frac{\sigma_i(\tilde{\hat{b}}_m)}{\sigma_i(\hat{b}_m)} \right] + \frac{\left[D_i - m_i(\tilde{\hat{b}}_m) \right]^2}{2\sigma_i^2(\tilde{\hat{b}}_m)} - \frac{\left[D_i - m_i(\hat{b}_m) \right]^2}{2\sigma_i^2(\hat{b}_m)} \end{aligned} \tag{3.29}$$

where $\hat{b}_m$ is the decoded information at the relay, and $\tilde{\hat{b}}_m$ stands for the flipped version of $\hat{b}_m$.

Recall the channel quality indicator M_i in (3.6), only a division following a substraction operation is needed once D_i is obtained at the relay; thus a rather simple structure will work for the design of the receiver. However, the implementation of the

LLR indicator will increase the receiver complexity. The MinMax-RS strategy based on indicator LLR is demonstrated to outperform the same strategy based on M by simulation in Section 3.6, with a relative complex receiver structure.

3.6 Simulation Results

In this section, the numerical results for the performance of the five cooperative TRPC strategies proposed above are presented. The simulation is carried out in the CM1 and CM8 channels defined by IEEE 802.15.4a standard, respectively. The parametric settings are the same as that mentioned in Section 3.1.3, and the system is assumed to be ISI free.

The performance comparisons between various methods under CM1 channel environment are shown in Fig. 3.6. Based on the channel quality indicator M, when the outage threshold ϱ is selected to be 0.2, the proposed WRC strategy is slightly better than the ORS scenario, and both of them are demonstrated to be more reliable than the RC case. MP-RS and MinMax-RS have similar performances, and they both outperform the other three cases, with about 2 dB gain over the RC case at BER $= 10^{-4}$. For the MP-RS case, the simulation result for the cooperative system without PNC is shown to have inferior performance to that with PNC, which demonstrates the effectiveness of PNC under the same data rate. As well, the performance of M and LLR indicator under MinMax-RS protocol are compared. From simulation, it is seen that LLR predicts the channel quality better than M does, with a slightly increase in the receiver complexity. Moreover, the analytical BER results of the M indicator based MinMax-RS strategy agree well with the simulation results, which validates our theoretical analysis.

The performance of different strategies under CM8 channel environment is shown

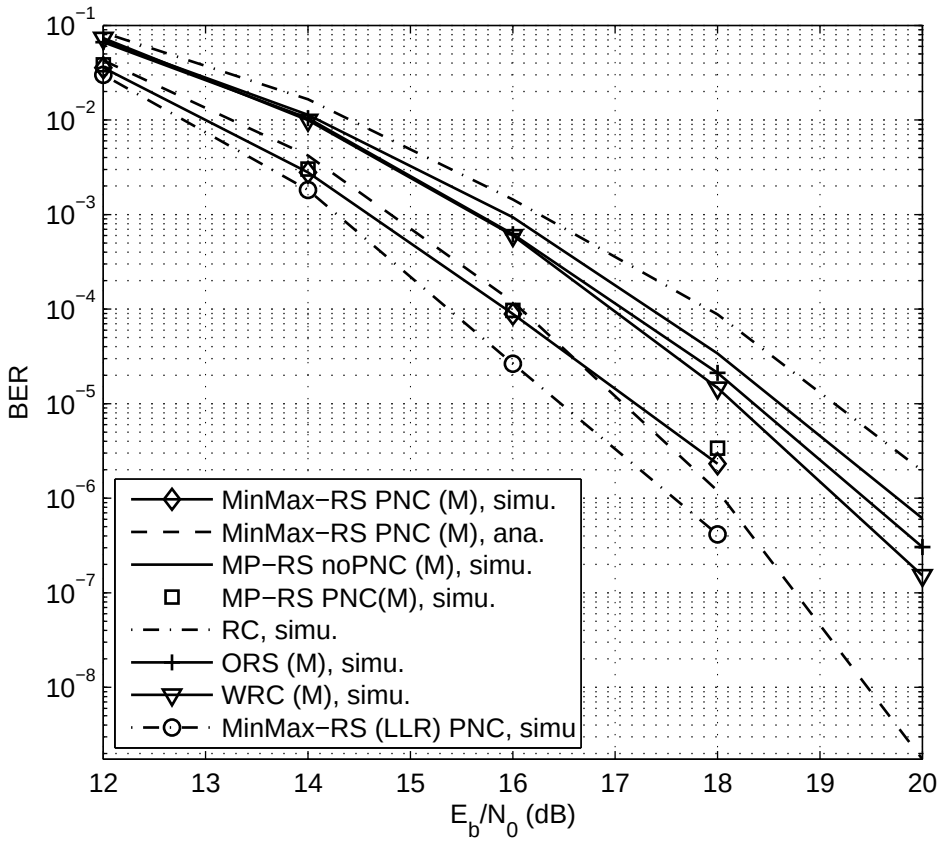

Figure 3.6: Simulation results for performance of various cooperative strategies under CM1 channel environment

in Fig. 3.7. It can be seen that under the highly dispersive environment, the system has a slightly better performance following the ORS strategy than the WRC case, versus the CM1 scenario. The MinMax-RS and MP-RS strategies still demonstrate the most robust performance among all the proposed cooperative strategies, and the LLR indicator based MinMax-RS strategy yield the best BER performance, the same as that in the CM1 case, indicating the effectiveness of the proposed relay selection.

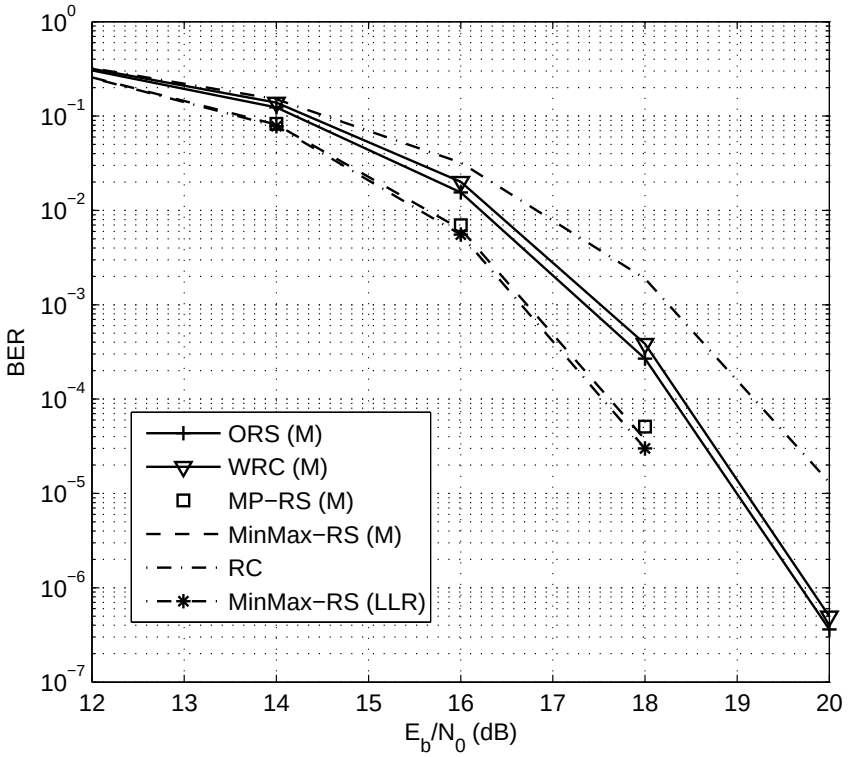

Figure 3.7: Simulation results for performance of various cooperative strategies under CM8 channel environment

Chapter 4

Shadowing Effects on Cooperative Relay Networks

In this Chapter, the scenarios when shadowing effects are taken into account in different hops of the cooperative network (as shown in Fig. 2.3) are considered. The CM1 and CM8 channel environments are investigated in Sections 4.2 and 4.3, respectively.

For the network topology under the CM1 channel environment, the cooperative strategies proposed in Chapter 3 are demonstrated to be useful from simulation when shadowing effects are considered in different hops of the network. And for the CM8 shadowing environments, a novel multipath channel based relay selection strategy (MC-RS) is proposed. Instead of the bit-by-bit relay selection strategies proposed in Section 3.2∼3.5, the MC-RS strategy only executes the relay selection once for each channel realization. Then a joint relay selection strategy (JRS) is introduced based on both the channel and bit level relay selection. The simulation results reveal that under the extremely dispersive channel environment, the JRS strategy can approach the BER performance of the bit level based MinMax-RS case.

4.1 Shadowing Effects in Wireless Communications

Due to user movements, the wireless radio channel is susceptible to the noise, interference and channel impediments, the unpredictable character of which make it challenging for the reliable high-speed communications. As it has been discussed in Section 2.1, the UWB channel can be briefly modeled by the large scale fading, shadowing (or medium scale fading), and small scale fading. The large scale fading mainly contributes to path loss, which is caused by the effects of the propagation channel as well as the dissipation of power radiated by the transmitter; the variation due to path loss occurs over very large distances (100-1000 meters). Shadowing is caused by the obstacles that absorb power between the transmitter and receive. Versus the path loss, the variation due to shadowing occurs over distances proportional to the length of the obstructing object (10-100 m in outdoor environments and less in indoor environments). The small scale fading is caused by the multipath signal components, and occurs over very short distances (on the order of signal wavelength) [2]. An illustration for the ratio of the received to transmit power (P_r/P_t) versus log-distance representing the three kinds of fading mentioned above can be found in Fig. 4.1.

4.1.1 Simplified Path Loss Model

The free space path loss model is the simplest model for signal propagation. It generally assumes that path loss is the same at a given transmit-receive distance, without consideration of the shadowing effects. The simplified path loss model is a function of distance (d) as

$$P_r = P_t K \left[\frac{d_0}{d}\right]^{\gamma}. \tag{4.1}$$

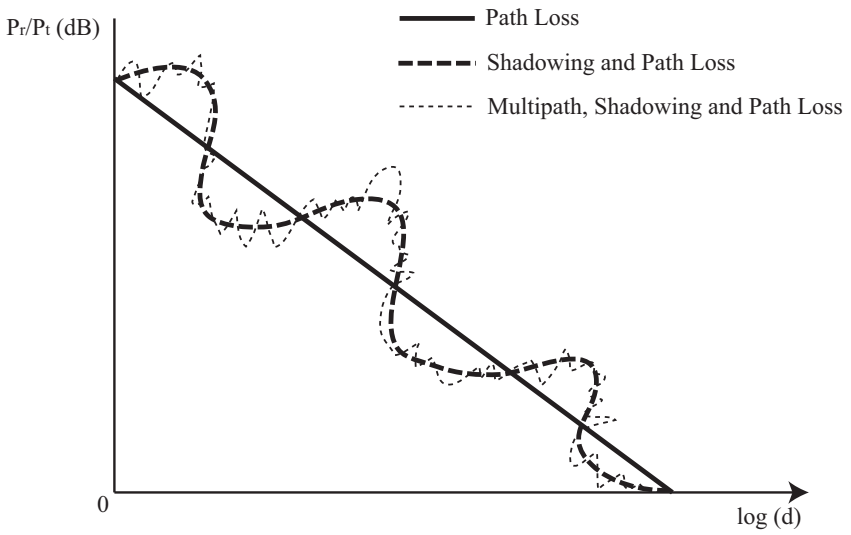

Figure 4.1: Shadowing effects on wireless channel model [2]

where P_r and P_t represents the received and transmit power, respectively, K depends on the antenna characteristics as well as the average channel attenuation, and is a unitless constant, γ is the path loss exponent depending on the propagation environment, and d_0 is a reference distance for the antenna far-field, which is typically assumed to be 1-10 m indoors and 10-100 m outdoors.

Furthermore, if the dB attenuation is adopted, then (4.1) becomes

$$P_r(dBm) = P_t(dBm) + K(dB) - 10\gamma \log_{10}\left[\frac{d}{d_0}\right], \tag{4.2}$$

or its substitute form as

$$\frac{P_r}{P_t}(dB) = 10\log_{10} K - 10\gamma \log_{10}\frac{d}{d_0}. \tag{4.3}$$

4.1.2 Shadowing Effects

Besides the path loss, shadowing effects will give rise to the random variation of the received power at a given distance due to the blockage from objects in the signal path. The blockage may attribute to the uncertainty of the location, size and the dielectric properties of the blocking objects, as well as the changes in reflecting surfaces and scattering objects that cause the random attenuation. A lognormal shadowing model is typically adopted for this additional attenuation [2].

As models for the path loss and shadowing are usually superimposed to capture the power fall off versus distance, (4.3) becomes (4.4) when the shadowing effects are taken into account, as

$$\frac{P_r}{P_t}(dB) = 10\log_{10} K - 10\gamma \log_{10}\frac{d}{d_0} + \psi_{dB}, \tag{4.4}$$

where ψ_{dB} is a zero mean Gaussian distributed random variable with variance $\sigma^2_{\psi_{dB}}$, whose corresponding linear mean (not in dB) distribution (ψ) can be written as

$$p(\psi) = \frac{\xi}{\sqrt{2\pi}\sigma_{\psi_{dB}}\psi} \exp\left[-\frac{(10\log_{10}\psi - \mu_{\psi_{dB}})^2}{2\sigma^2_{\psi_{dB}}}\right], \tag{4.5}$$

where $\xi = 10\ln 10$, $\psi_{dB} = 10\log_{10}\psi$, and $\mu_{\psi_{dB}}$ and $\sigma_{\psi_{dB}}$ represent the mean and standard deviation of ψ_{dB} in dB, respectively.

4.1.3 Shadowing Effects on UWB channels

As a particular class of the wireless channels, the shadowing effects on the UWB channels can be analyzed in the same way. Thus for a single UWB channel realization,

(2.10) will be amended by (4.6) considering the shadowing effects as [33]

$$h(t) = \psi \sum_{k=0}^{K-1} \alpha_k \delta(t - \tau_k), \tag{4.6}$$

where the shadowing term ψ is characterized by

$$20 \log_{10} \psi \propto N\left(0, \sigma_S^2\right), \tag{4.7}$$

and where σ_S for different UWB channel models can be found in Table 4.2.

4.2 Cooperative Relay Networks under CM1 Shadowing Channels

4.2.1 Introduction of the UWB 4a Channel Classifications

According to the IEEE 802.15.4a standard, the UWB channels have been divided into eight classes (CM1-CM8) due to different environments as in Table 4.1 [34].

Channel Model	**Environment**
CM1	Residential LOS
CM2	Residential NLOS
CM3	Indoor Office LOS
CM4	Indoor Office NLOS
CM5	Outdoor LOS
CM6	Outdoor NLOS
CM7	Industrial LOS
CM8	Industrial NLOS

Table 4.1: UWB channel classifications

Based on the classification, parameterizations are done by [28] according to measurement results in reality. The measurement range and frequency for each UWB

channel model can be found from Table 4.2. Moreover, the shadowing standard deviation for each channel model from the measured results are also listed out in the table, in order to give a reference to the simulations for the rest of this chapter.

Channel Model	**Measurement Range (m)**	**Measurement Frequency (GHz)**	**Shadowing Standard Deviation** ($\sigma_S(dB)$)
CM1	7-20	10	2.22
CM2			3.51
CM3	3-28	2-8	1.9
CM4			3.9
CM5	5-17	3-6	0.83
CM6			2
CM7	2-8	3.1-10.6	6
CM8			6

Table 4.2: Parameterizations for UWB channel models

As it has been mentioned in Table 4.1, CM1 channel model stands for the residential line of sight (LOS) environment, which is the typical UWB channel model. The building structures of residential environments are characterized by small units, with indoor walls of reasonable thickness [35]. And the environments are critical for "home networking", linking different appliances, as well as safety (fire, smoke) sensors over a relatively small area. Thus the CM1 channel model is selected as a representative environment to analyze the proposed cooperative strategies in the following subsection.

4.2.2 Shadowing Effects on the Cooperative Network

In this section, it is assumed that all the hops ($\mathbf{h}_1$, $\mathbf{h}_2$, $\mathbf{h}_3$, and $\mathbf{h}_4$) in the cooperative network (as shown in Fig. 2.3) conform to the CM1 channel model. Scenarios when shadowing are considered in different hops of the network are investigated. Four representative cases, that is, shadowing existing in $\mathbf{h}_1$, $\mathbf{h}_1$ and $\mathbf{h}_2$, $\mathbf{h}_1$ and $\mathbf{h}_4$, and all

of the four hops are discussed. Simulations are taken following the five cooperative strategies proposed in Chapter 3 using indicator M.

As it has been discussed in Section 4.1, for a single hop $\mathbf{h}_i$, channel in (2.10) becomes $\mathbf{h}_i' = \psi \mathbf{h}_i$. Thus BER in (2.20) becomes (4.8) when shadowing effects are included.

$$P(e|\mathbf{h}, \psi) = Q\left(\frac{\psi^2\left(-m_D(-1) + m_D(+1)\right)}{\sqrt{\psi^2\left(\sigma_{23}^2(-1) + \sigma_{23}^2(+1)\right) + 2\sigma_4^2}}\right) \tag{4.8}$$

And the PDF of the zero mean Gaussian noise $f_n(x)$ ($f_n(x) \sim CN(0, \sigma_D^2(b_m))$) in (3.24) changes into

$$\tilde{f}_n(x|\psi) = \frac{1}{\sqrt{2\pi}\sqrt{\psi^2\sigma_{23}^2(b_m) + \sigma_4^2}} e^{-\frac{x^2}{2(\psi^2\sigma_{23}^2(b_m) + \sigma_4^2)}}. \tag{4.9}$$

Then similar procedures could be adopted for the system BER analysis as those have been done for the corresponding scenario without shadowing effects in Section 3.5.

4.2.3 Simulation Results under CM1 Shadowing Channel Environment

In this section, the simulation results from different cooperative strategies under the CM1 shadowing environment are presented.

Fig. 4.2 simulates the case when shadowing effects are only considered in $\mathbf{h}_1$. It is seen that the analytical result agrees well with simulation for the MinMax-RS strategy, demonstrating the validity of the theoretical derivation. Fig. 4.3 represents the case when shadowing are included in both $\mathbf{h}_1$ and $\mathbf{h}_2$, and the scenario when shadowing effects are taken into account in all the four hops is shown in Fig. 4.4. From the figures, it is observed that the proposed MinMax-RS strategy demonstrates the most robust performance under all these circumstances, consistent with the scenarios

without shadowing.

When shadowing effects are considered in two symmetric channels (e.g. $\mathbf{h}_1$ and $\mathbf{h}_4$), which are not connected directly by the relay, the simulation result is shown in Fig. 4.5. The figure shows that when E_b/N_0 is relative low, the MinMax-RS strategy is the most reliable one; however, when E_b/N_0 becomes larger than around 16 dB, the ORS scheme results in the lowest BER, which may contribute to the diversity brought by the second relay.

4.3 Cooperative Relay Networks under CM8 Shadowing Channels

In this section, the highly dispersive environments following the CM8 channel model are investigated, where shadowing effects become substential.

In Chapter 3, the idea of channel quality indicator is introduced, where channel selection is done from bit to bit at the relay. And the previous simulation results have demonstrated the effectiveness of the channel quality detection. In this section, a multipath channel based relay selection strategy that can greatly extenuate the workload at relay is introduced, according to which the cooperative relay is selected once for each channel realization. A joint relay selection strategy that balances on the system performance and relay overhead is further proposed, and the BER performance of the JRS strategy is testified to approach the bit-by-bit selection schemes from simulation under the CM8 shadowing environment.

4.3.1 Introduction of the UWB CM8 Channel Model

As been characterized by huge enclosures (e.g., factory halls), which are filled with a large number of metallic reflectors, the CM8 channel model for the industrial NLOS

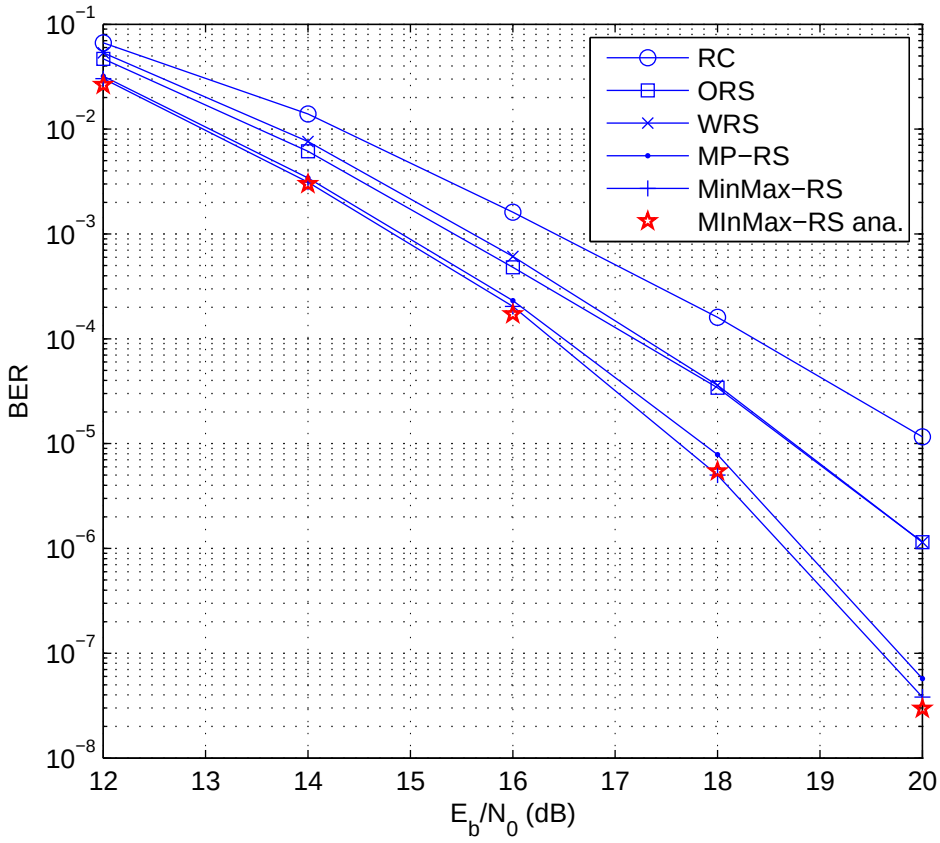

Figure 4.2: Simulation results for performance of different cooperative strategies when shadowing effects are considered in $\mathbf{h}_1$ under the CM1 channel environment

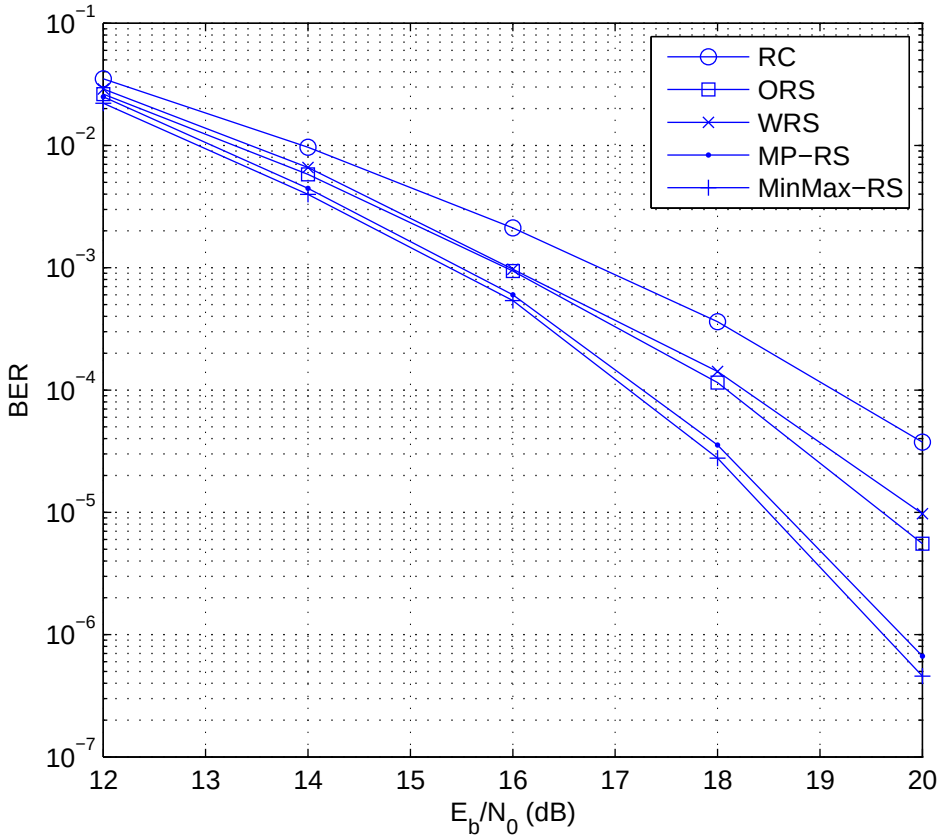

Figure 4.3: Simulation results for performance of different cooperative strategies when shadowing effects are considered in both $\mathbf{h}_1$ and $\mathbf{h}_2$ under the CM1 channel environment

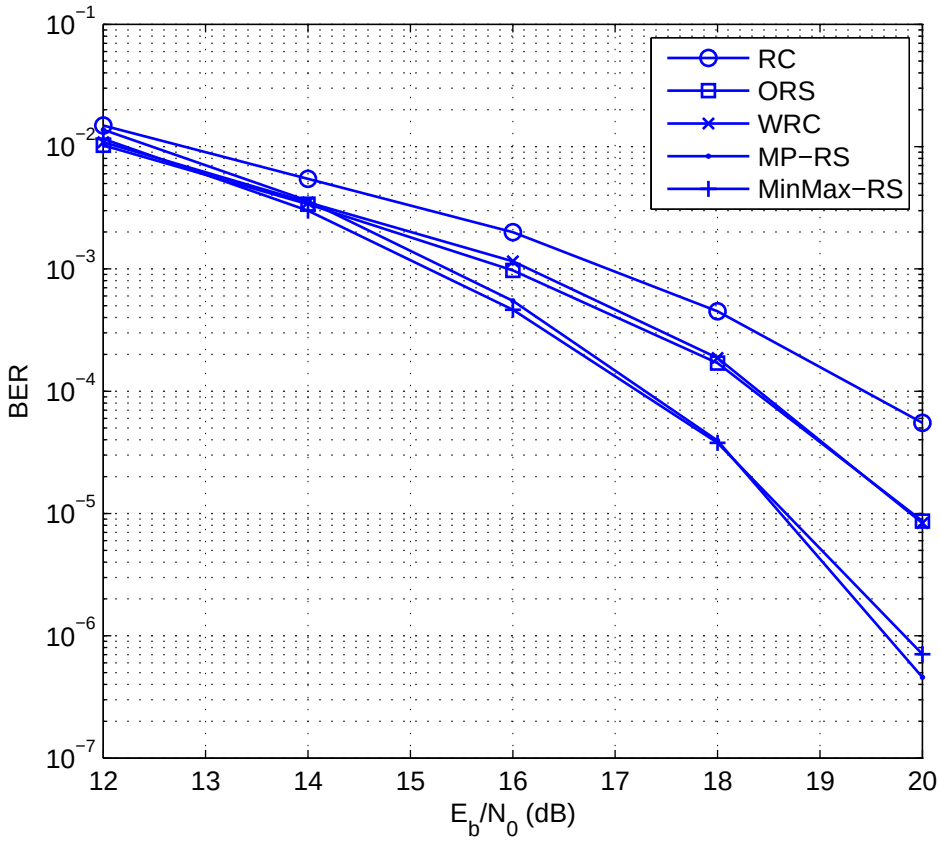

Figure 4.4: Simulation results for performance of different cooperative strategies when shadowing effects are considered in all four hops under the CM1 channel environment

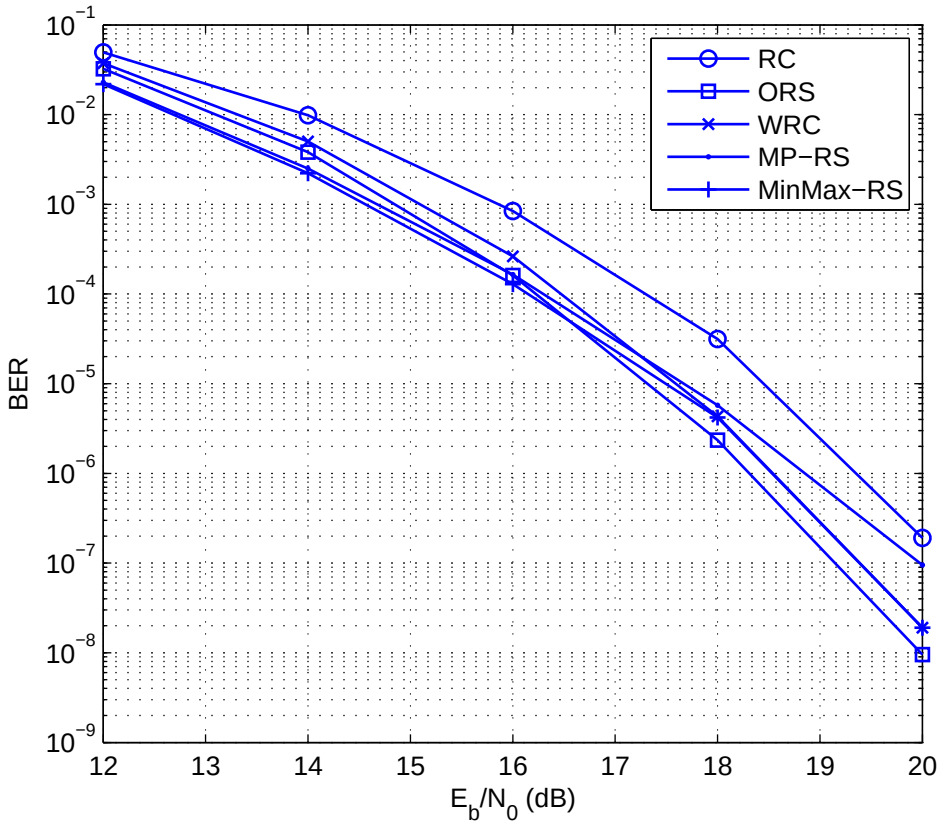

Figure 4.5: Simulation results for performance of different cooperative strategies when shadowing effects are considered in both $\mathbf{h}_1$ and $\mathbf{h}_4$ under the CM1 channel environment

environment is anticipated to experience severe multipaths [35]. Hence the shadowing effects become extremely significant under the CM8 channel environment. It is demonstrated by the measurement results in Table 4.2, where σ_S becomes 6, much larger than the other environments.

Under the industrial environment, scattering and reflections in the presence of large size metallic objects and numbers of inductive loads, generate plenty of resolvable multipath components (MPCs) and lead to a dense power delay profile (PDP). It makes the dense multipath as the most significant characteristic of the UWB CM8 channel model. As a result of the multipath propagation, the PDP for CM8 channel appears with only one single cluster which first rises to a maximum and then drops off, which means the differences of the time delay in the travel time between multipath signals own a unique local maximum point at a certain value, showing that the first ray is not carrying the largest amount of energy. The maximum of the PDP may be several tens of nanoseconds after the arrival of the first component, thus the common approximation of a single exponential PDP does not hold at all in those cases [36].

Moreover, in contrast to the Poisson distributed cluster and ray arrival times with exponential arrival rates in the other environments, the channel impulse response for UWB CM8 channel model appears as a tapped delay line model with Nakagami distribution for small scale fading [37], as we have discussed in (2.8)-(2.9).

In conclusion, in contrast to the other UWB channel models, the CM8 channel experiences extremely dense multipaths; in other words, almost all resolvable delay bins contain significant energy. The relay cooperative strategies for the CM8 channel environment with shadowing effects taken into account are investigated in the following subsections.

4.3.2 Multipath Channel Based Relay Selection (MC-RS)

For the extremely dispersive CM8 shadowing environment as been discussed in Section 4.3.1, the signal-and-noise and noise-noise products ($\mathbf{D}_2 + \mathbf{D}_3 + \mathbf{D}_4$ in between (2.16)) may become dominant in D. Thus D has a higher probability to fall into the wrong region of the decision threshold. In view of this situation, two other cooperative strategies, namely the multipath channel based relay selection strategy (MC-RS) and joint relay selection strategy (JRS), are introduced in this and next subsections, which will achieve a tradeoff between the hardware complexity and BER performance.

The idea of the MC-RS strategy is to select the channel with better quality according to C, which is defined as

$$C_i = \frac{2E_i}{\sigma_i}, \tag{4.10}$$

where E_i is given in (3.7) conditioned on channel $\mathbf{h}_i$, and $\sigma_i = \sqrt{\sigma_i^2(+1) + \sigma_i^2(-1)}$. E_i and σ_i can be estimated from the pilot sequences as been mentioned in Section 3.2.1, and can be viewed as the statistical properties of a certain channel realization $\mathbf{h}_i$. C can represent the channel quality; and the heavier the shadowing is, the smaller C will become.

Opposite to both the M and LLR indicators, which can detect the transmit reliability on the bit level, C represents the channel quality for each channel realization. That is, with the use of the C indicator, the noise variation in each bit transmission is neglected in the detection, and hence reducing the relay overhead.

In order to analyze the multipath channel based relay selection in the cooperative network, we first recall the prototype of the TWR system as shown in Fig. 4.6.

N_1 and N_3 exchange information with the help of the relay node N_2, where PNC

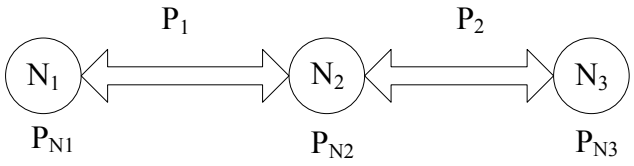

Figure 4.6: Prototype of a TWR system

is done towards the received bits in the MA phase. P_1 and P_2 denotes the BER of the symmetric channel between N_1-N_2 and N_3-N_2, respectively. Thus the BER at N_2 after PNC becomes

$$P_{N_2} = 1 - P_1P_2 - (1 - P_1)(1 - P_2) = P_1 + P_2 - 2P_1P_2. \tag{4.11}$$

Then BER at the source nodes N_1 and N_3 can be expressed as

$$\begin{aligned} P_{N_1} &= P_1 + P_{N_2} - 2P_1P_{N_2} \\ P_{N_3} &= P_2 + P_{N_2} - 2P_2P_{N_2}. \end{aligned} \tag{4.12}$$

As it has been mentioned above, the two users want to exchange the same amount of information. Thus the performance of the TWR system P_{TWR} can be evaluated from the average of the error probabilities at N_1 and N_3, that is

$$\begin{aligned} P_{TWR} &= \frac{1}{2}(P_{N_1} + P_{N_3}) \\ &= \frac{1}{2}(P_1 + P_2) + P_{N_2} - P_{N_2}(P_1 + P_2) \\ &= \frac{3}{2}(P_1 + P_2) - 4P_1P_2 - P_1^2 - P_2^2 + 2P_1^2P_2 + 2P_1P_2^2. \end{aligned} \tag{4.13}$$

When the two hops in the TWR system are under similar environment ($P_1 \approx P_2$),

then P_{TWR} in (4.13) can be approximated by $\tilde{P}_{TWR}$ as

$$\tilde{P}_{TWR} \approx 3P_1 - 6P_1^2 + 4P_1^3. \tag{4.14}$$

As P_1 and P_2 are generally less than 10^{-1} for the environment which this thesis is aiming at, (and often far smaller than that for majority cases), it is obvious that the second and third terms are much smaller than the first term. Then the value of $\tilde{P}_{TWR}$ can be roughly estimated by $3P_1$. That is, $\tilde{P}_{TWR}$ can be reflected by a single hop (P_1 or P_2) channel condition under the similar assumptions.

Otherwise, if the two hops experience significantly different environments, e.g. $P_1 \gg P_2$, which is the most representative scenario for the CM8 shadowing networks, P_{TWR} in (4.13) can be rewritten by $\breve{P}_{TWR}$ as

$$\breve{P}_{TWR} = P_1(\frac{3}{2} - 4P_2 + 2P_2^2) - P_1^2(1 - 2P_2) + \frac{3}{2}P_2 - P_2^2. \tag{4.15}$$

In this case, the hop under worse channel condition (with larger P_i, i=1,2) becomes the dominant part to evaluate the BER of the TWR system.

From both cases above, it is seen that the quality of a TWR network is mainly limitted by the condition of the worse one from the two hops. Moreover, as the indicator C_i can reflect P_i, the TWR link with larger minimum C_i has higher reliability in the communication.

The cooperation mode of the MC-RS strategy is the same with that in the MinMax-RS one, whereas it has different relay selection criterions. In the MC-RS strategy, instead of $Z^1 = min(M_1, M_2)$ and $Z^2 = min(M_3, M_4)$, $\bar{Z}^1 = min(C_1, C_2)$ and $\bar{Z}^2 = min(C_3, C_4)$ are defined, and the relay selection is executed accordingly, where the assigned cooperating relay R_c will keep broadcasting for a whole transmit package. The performance of the MC-RS strategy is shown to approach that following

the bit-by-bit selection schemes from the simulation results shown in Section 4.3.4.

4.3.3 Joint Relay Selection (JRS) Cooperative Strategy

In this subsection, another cooperative strategy combining both the channel and bit level selection is introduced, namely the JRS strategy. Following the JRS strategy, the system attempts to turn into a channel level based selection mode to save the receiver overhead at relays when the network is exposed to poor channel conditions; and when the channel condition is demonstrated to be acceptable, it will turn into the bit-by-bit selection mode in order to strengthen the system reliability.

In the JRS strategy, a threshold $thre$ is first defined for C. When $C \geq thre$, the channel is viewed as in good quality; otherwise, it is assumed to experience severe shadowing. Then, relays select to participate in the bit level channel quality detection according to C: when both of the four hops are in good quality, the MinMax-RS protocol is adopted to finish communication in the BC phase; otherwise, when at least one hop is exposed to poor channel conditions, the broadcasting relay is chosen once for a whole transmit package according to the MinMax criterion as: R_1 is chosen when $\bar{Z}^1 \geq \bar{Z}^2$; otherwise, R_2 is chosen to broadcast in the BC phase.

By this JRS strategy, a balance can be reached between the overhead and reliability of the system. The simulation results when the shadowing effects are included in the CM8 network are shown in Section 4.3.4. It reveals that the JRS strategy can slightly improve the performance of the MC-RS case, and both of them can approach the MinMax-RS strategy with channel quality indicator LLR under the CM8 shadowing environment, with a more robust performance than the plain RC scenario.

4.3.4 Simulation Results under CM8 Shadowing Channel Environment

In this subsection, simulation results for different cooperative strategies are presented, under the CM8 channel environment with shadowing effects taken into account.

Fig. 4.7 shows the case when shadowing effects are considered in only one hop ($\mathbf{h}_1$) of the network under the CM8 channel environment. The JRS strategy is simulated when the threshold *thre* is chosen to be 3 and 4 respectively. Fig. 4.8 represents the scenario that shadowing effects are included in two hops with direct connection (e.g., $\mathbf{h}_1$ and $\mathbf{h}_2$). Fig. 4.9 is for the situation that shadowing effects are taken into account in two hops without direct connection (e.g., $\mathbf{h}_1$ and $\mathbf{h}_4$). And when all the channels are exposed to shadowing effects, the simulation result can be found in Fig. 4.10.

The figures reveal that under all the network assumptions, the JRS strategies based on M and LLR indicators give similar performance, they both slightly outperform the plain MC-RS case. And they can approach the performance of the LLR based MinMax-RS strategy when *thre* is properly chosen. If *thre* is too large, the JRS strategy will become the channel based selection; or if it is too small, it will become the corresponding bit-by-bit selection strategy.

Thus by combining both the channel and bit-by-bit level selection, it can help to make the communication more reliable, and lighten the relay detection overhead at the same time.

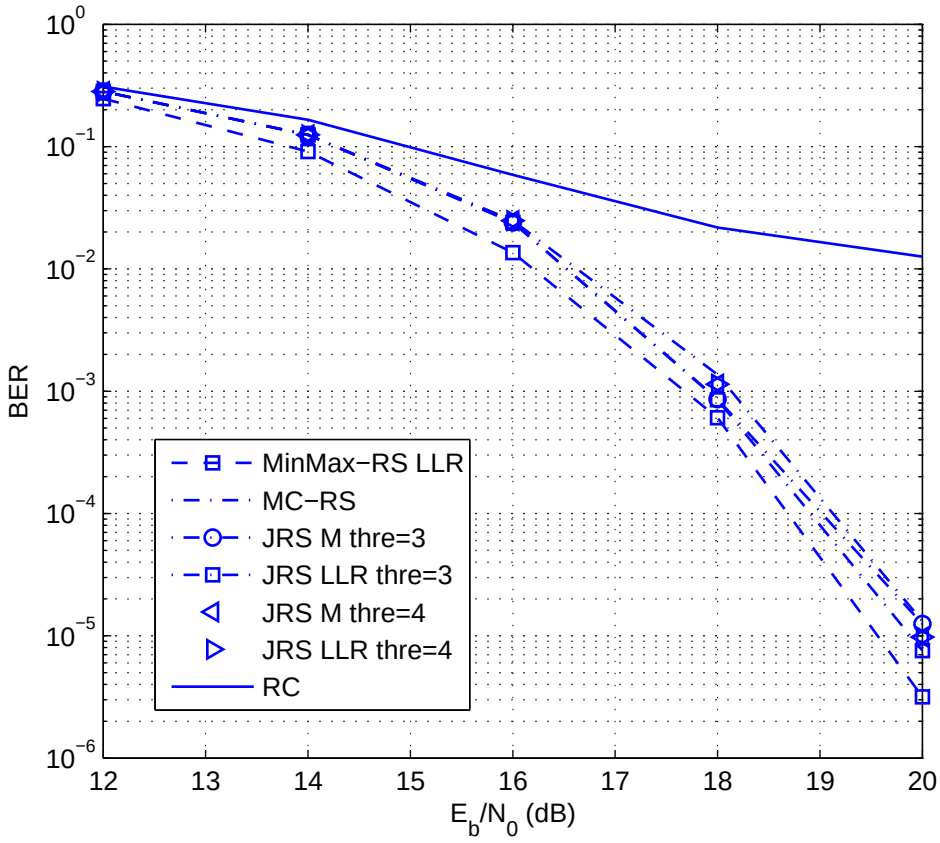

Figure 4.7: Simulation results for performance of different cooperative strategies when shadowing effects are considered in $\mathbf{h}_1$ under the CM8 channel environment

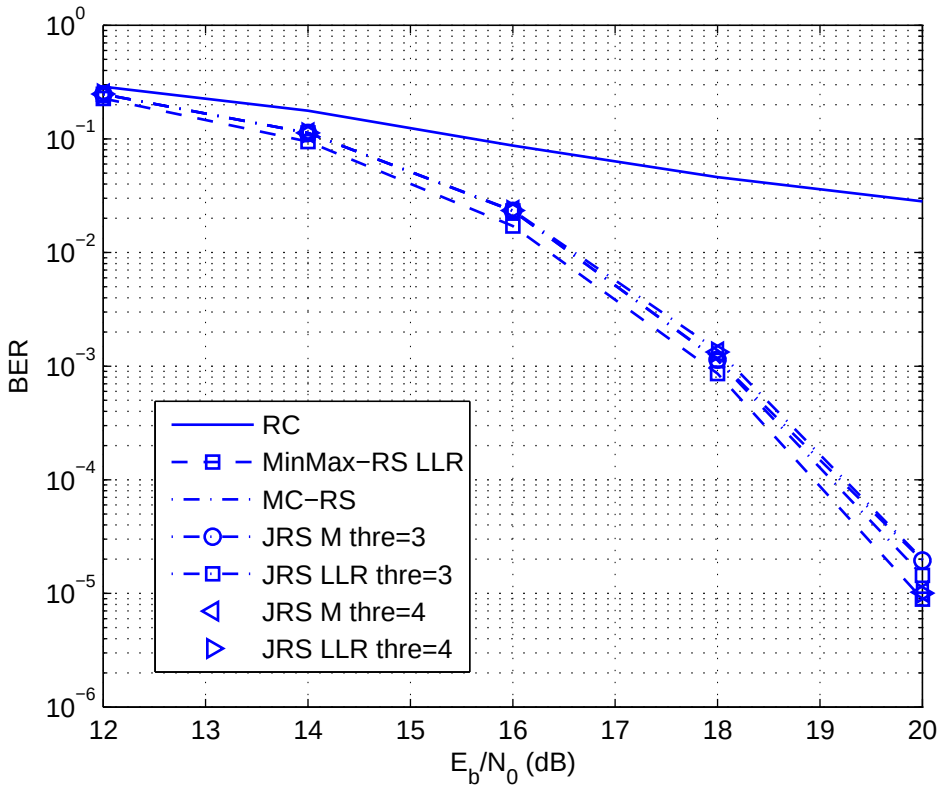

Figure 4.8: Simulation results for performance of different cooperative strategies when shadowing effects are considered in both $\mathbf{h}_1$ and $\mathbf{h}_2$ under the CM8 channel environment

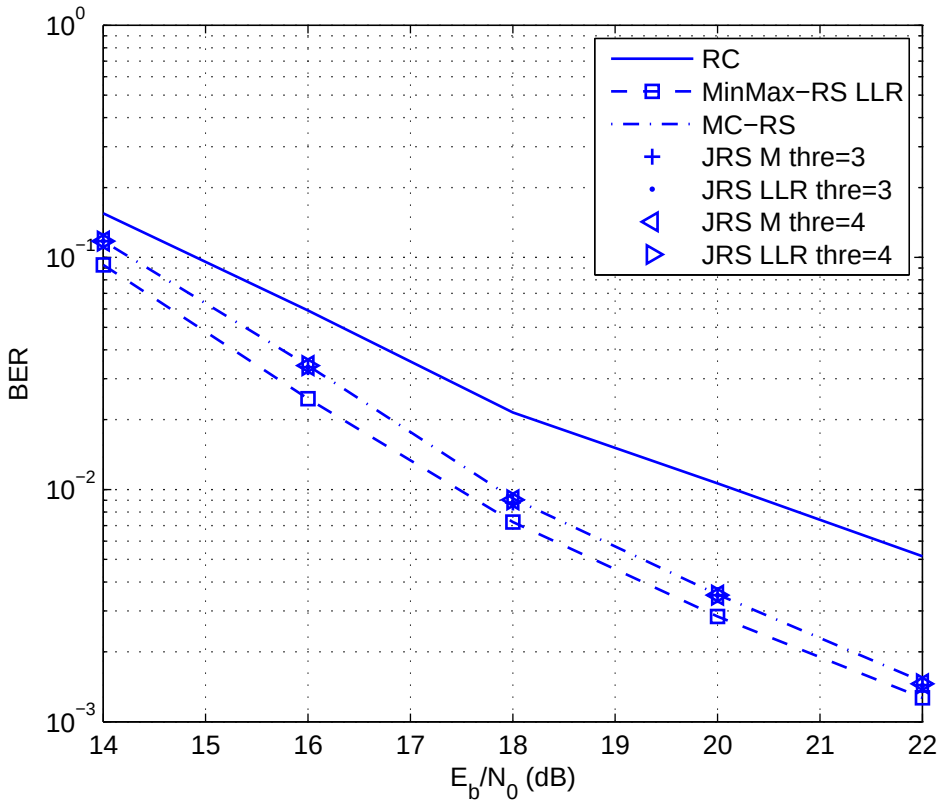

Figure 4.9: Simulation results for performance of different cooperative strategies when shadowing effects are considered in both $\mathbf{h}_1$ and $\mathbf{h}_4$ under the CM8 channel environment

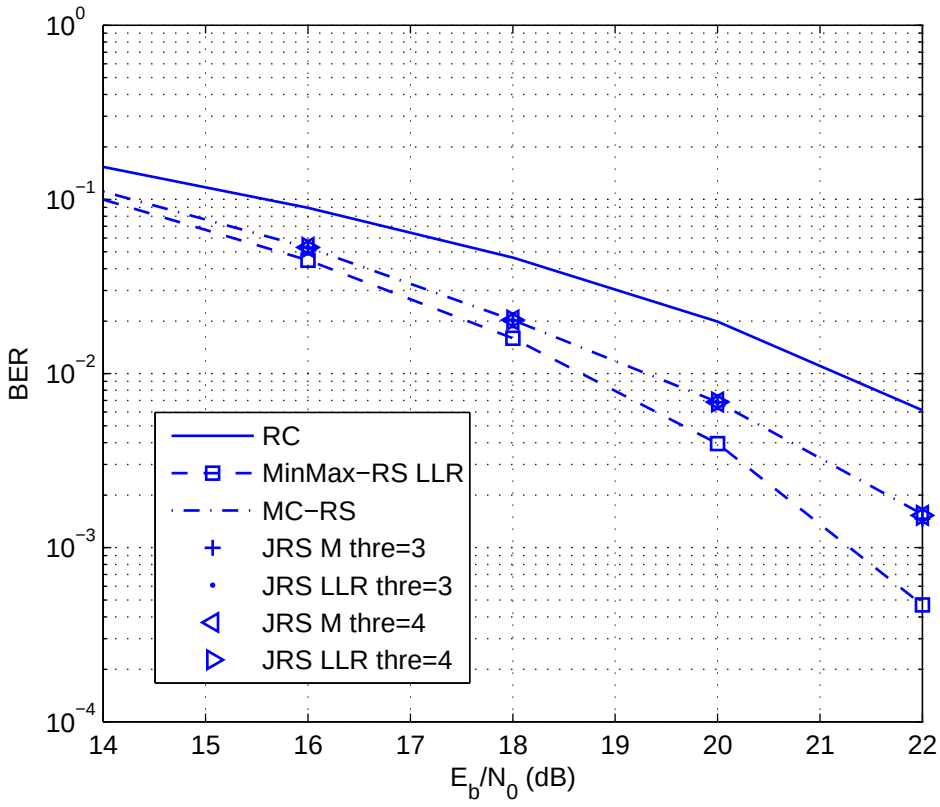

Figure 4.10: Simulation results for performance of different cooperative strategies when shadowing effects are considered in all four hops under the CM8 channel environment

Chapter 5

Power Allocation Strategy for Two-way-relay Systems

In this chapter, the power allocation strategy for a TRPC two-way-relay (TWR) system is introduced following the IEEE 802.15.4a channel model. The SNR is derived for a UWB TRPC system first. Then its corresponding PDF model is obtained by curve fitting of the sampled data generated through Monte Carlo experiments. Based on that, a amended SNR distribution is further given when different transmit power and pathloss coefficients are taken into consideration. At last, the outage probability function for the TRPC system is derived, and a numerical optimization algorithm is presented to find the proper power allocation strategy leading to the minimum system outage, restricted by the total transmit power from all the three peer nodes. The proposed power allocation strategy is compared with three other straight forward schemes through simulation. And the results validate the reliability of the proposed strategy.

5.1 Two-way-relay (TWR) System Model

5.1.1 Cooperative TWR System Structure

Recall a three node TWR system model as been mentioned in Fig 4.6. It can be assumed that one user S_1 has a constant distance from relay R, represented by d_1 in Fig. 5.1, without loss of generality. And its peer node S_2 is a roaming user, the distance between S_2 and R (d_2) varies when S_2 moves around the relay.

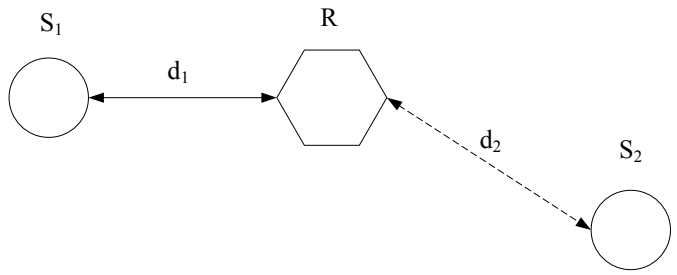

Figure 5.1: Cooperative TWR system model

5.1.2 IEEE 802.15.4a PathLoss Model

Recall the pathloss model introduced in Section 4.1.3, (4.3) can be rewritten as

$$PL(d) = PL_0 + 10\gamma \log_{10} \frac{d}{d_0} \tag{5.1}$$

where the reference distance d_0 is set to 1 m, and $PL_0 = 10 \log_{10} K$. Denote $d_2 = a \times d_1$, and the linear form of the pathloss $\overline{PL}(d)$ has $\overline{PL}(d_2) = l \times \overline{PL}(d_1)$, where l can be expressed as

$$l = \frac{\overline{PL}(d_2)}{\overline{PL}(d_1)} = 10^{\frac{\overline{PL}(d_2) - \overline{PL}(d_1)}{10}} = a^{\gamma}. \tag{5.2}$$

In this chapter, a TWR system as shown in Fig. 5.1 is investigated, where S_1 and

S_2 exchanges information with the help of relay. When S_2 roams, the optimum power allocation strategy for the TWR system is discussed, the transmit powers at S_1, R and S_2 are reallocated in order to minimize the system outage probability.

5.2 Outage Probability for TWR Systems

5.2.1 SNR Analysis for a Single hop TRPC Transmission

In this section, the SNR performance for a single hop UWB channel realization using TRPC is analyzed, and the pathloss coefficient is considered additionally.

As been proved in [38], the conditional mean of $\Re\{D\}$ (D given in (2.14)) can be expressed as

$$E[\Re\{D\}|b_i] = b_i \cdot U + V \tag{5.3}$$

where b_i is the transmit signal, U and V are given by

$$\begin{aligned} U &= \frac{E_b}{2N_r}\int_{T_1}^{T_2} |v(t-T_d)|^2\, dt + \Re\left[\frac{E_b}{2N_r}\int_{T_1}^{T_2} v(t)\cdot v^*(t-2T_d)dt\right] \\ V &= \frac{E_b}{2N_r}\int_{T_1}^{T_2} [v(t)\cdot v^*(t-T_d) + v(t-T_d)\cdot v^*(t-2T_d)]dt, \end{aligned} \tag{5.4}$$

$$\begin{aligned} v(t) &\triangleq w(t) * h(t) = \sum_{m=0}^{N_r} g(t-2mT_d) * h(t) \\ &= \sum_{m=0}^{N_r-1}\sum_{k=0}^{K-1} \alpha_k \cdot g(t-2mT_d-\tau_k), \end{aligned} \tag{5.5}$$

where $w(t)$ is a cluster only composed of reference pulses.

Thus, for each channel realization, SNR for the TRPC can be defined as

$$SNR \triangleq \frac{U^2}{\sigma^2(D)} \tag{5.6}$$

In Chapter 3, the bit-by-bit relay selection methods are introduced, where proper strategies are selected according to the detection at relays. In this chapter, in order to reduce the burden of the system, the transmit power at each node is allocated according to the location of S_2 instead of the channel quality detection. It means that for a certain pair of d_1 and d_2 in Fig. 5.1, the transmit power at the three nodes are related to the statistical channel environment only.

Because of the complexity lying in the channel modeling as well as autocorrelation caused by the TRPC detection, it is unrealistic to derive a closed form PDF expression for SNR in a TRPC UWB system. Thus the approximation of SNR distribution is investigated instead. It is found from Monte Carlo experiments that SNR conforms to the Loglogistic distribution under the CM1 channel environment, which is modeled as

$$f_{LOG}(x;\alpha,\beta) = \frac{(\beta/\alpha)\,(x/\alpha)^{\beta-1}}{\left[1+(x/\alpha)^{\beta}\right]^2} \quad (x>0;\alpha>0,\beta>0). \tag{5.7}$$

To test the goodness of this fit, the Kolmogorov−Smirnov (KS) statistical test is adopted. It is defined as the maximum value of the absolute difference between the two CDFs from simulation and approximation [39]. The Monte Carlo experiment is taken from 1000 CM1 channel realizations, when E_b/N_0 equals 22 dB. The PDF for SNR from simulation and its corresponding Loglogistic approximation are shown in Fig. 5.2, with $\alpha = 50.2289$ and $\beta = 7.4187$. The fit value between the simulation and approximation comes out to be 0.0444 following the KS test.

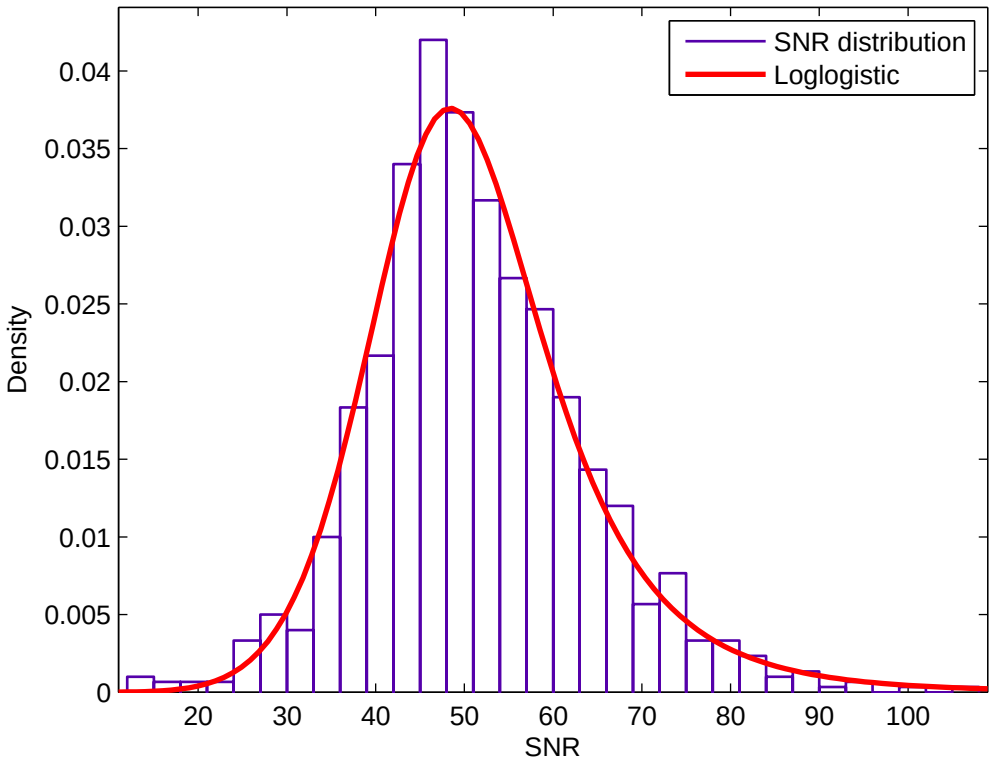

Figure 5.2: SNR distribution from Monte Carlo experiments for a 1000 CM1 channel set ($\frac{E_b}{N_0}$ =22 dB)

Apart from the CM1 channel realization, the scenario for CM2 channels is also investigated. From the Monte Carlo experiments, it is found that SNR follows Gamma distribution as (5.8) for the CM2 channel environment, versus the Loglogistic distribution for CM1 channel.

$$f_{GAMMA}(x;k,\theta) = x^{k-1}\frac{e^{-x/\theta}}{\theta^k\Gamma(k)} \qquad (x>0;k,\theta>0) \tag{5.8}$$

where $\Gamma(k) = (k-1)!$. Fig. 5.3 shows the Gamma approximation of the SNR distribution. When E_b/N_0 equals 22 dB, the scale parameter θ and shape parameter k are 3.2846 and 16.0698, respectively. The largest difference in the CDFs between simulation and approximation is 0.0138 given by the KS fitness test.

Furthermore, for a given E_b/N_0 at the transmitter, SNR given in (5.6) can be derived as

$$\begin{aligned} SNR &= \frac{\frac{E_b^2}{N_0^2}\left[\frac{1}{2N_r}\int_{T_1}^{T_2}|v(t-T_d)|^2dt + \Re\left[\frac{1}{2N_r}\int_{T_1}^{T_2} v(t)*v^*(t-2T_d)dt\right]\right]^2}{\frac{E_b}{N_0}\mathrm{Var}\left[\mathbf{S\text{-}N}\right] + \mathrm{Var}\left[\mathbf{N\text{-}N}\right]} \\ \mathbf{S\text{-}N} &= \sqrt{\frac{1}{2N_r}}\int_{T_1}^{T_2}\tilde{q}(t)\tilde{n}^*(t-T_d)dt + \sqrt{\frac{1}{2N_r}}\int_{T_1}^{T_2}\tilde{q}^*(t-T_d)\tilde{n}(t)dt \\ \mathbf{N\text{-}N} &= \int_{T_1}^{T_2}\tilde{n}(t)\tilde{n}^*(t-T_d)dt \end{aligned} \tag{5.9}$$

where $\tilde{q}(t) = \int_{k=0}^{K-1}\alpha_k g(t-\tau_k)$, and $\tilde{n}(t)$ is the normalized additive Gaussian noise.

As E_b/N_0 gets larger, the noise-noise term ($\mathrm{Var}\left[\mathbf{N\text{-}N}\right]$) becomes negligible. Thus, with the scaling of the transmit power, e.g. $E_b' = mE_b$, the SNR can be approximated by

$$SNR(E_b') \approx mSNR(E_b). \tag{5.10}$$

At the mean time, the Loglogistic distribution for CM1 channel in (5.7) changes to $f_{LOG}(x; m\alpha, \beta)$.

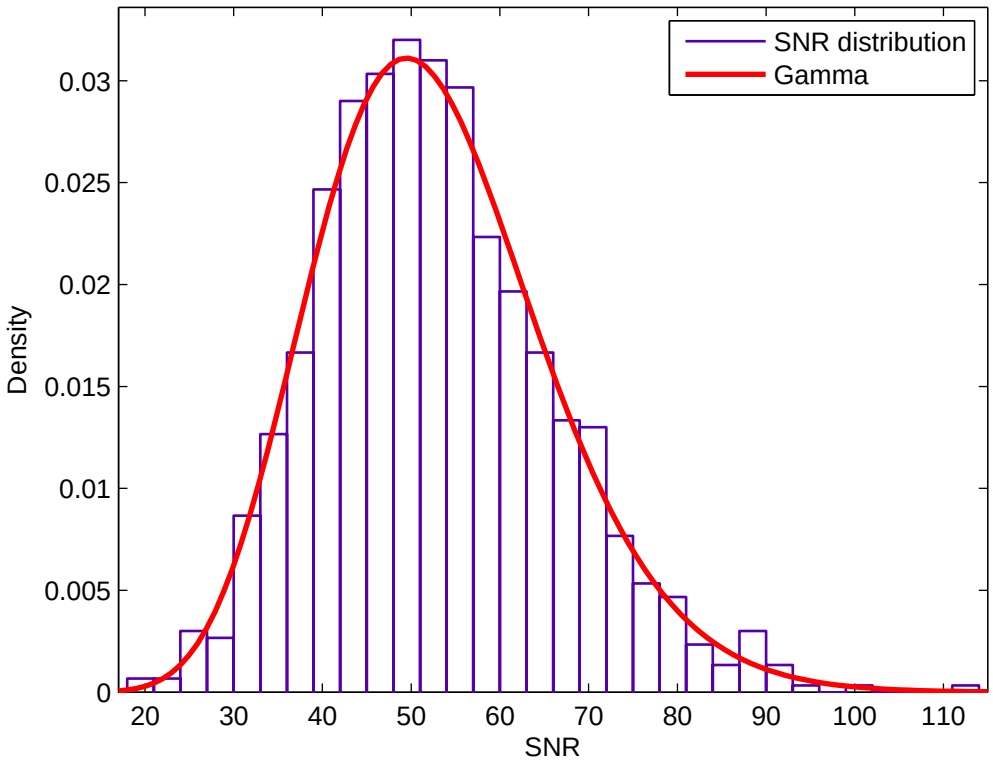

Figure 5.3: SNR distribution from Monte Carlo experiments for a 1000 CM2 channel set ($\frac{E_b}{N_0}$ =22 dB)

Similar analysis will be given if the pathloss effect is considered. Recall the roaming of S_2, then

$$SNR(d_2) \approx l^2 SNR(d_1). \tag{5.11}$$

5.2.2 Outage Probability for the TWR Systems

In this subsection, the outage probability performance for a TWR system is investigated, based on the approximated SNR distribution given in Section 5.2.1.

For a single hop of the TRPC transmission, an outage is defined as the scenario when SNR is lower than a threshold γ_0. Then its outage probability $\dot{P}$ can be calculated as (5.12),

$$\begin{aligned} \dot{P} &= F(SNR < \gamma_0) \\ &= \int_0^{\gamma_0} f(x;\alpha,\beta)dx \\ &= \frac{1}{1+\left(\frac{\gamma_0}{\alpha}\right)^{-\beta}} \end{aligned} \tag{5.12}$$

where $f(x;\alpha,\beta)$ is given in (5.7) for the CM1 channel environment.

For the TWR system shown in Fig. 5.1, outage happens if there is an outage existing in each of the four hop transmissions ($S_1 \to R : \dot{P}_1, S_2 \to R : \dot{P}_2, R \to S_1 : \dot{P}_3$ and $R \to S_2 : \dot{P}_4$). Thus the outage probability of the whole system (P_{out}) is defined as

$$P_{out} = 1 - (1-\dot{P}_1)(1-\dot{P}_2)(1-\dot{P}_3)(1-\dot{P}_4). \tag{5.13}$$

5.3 Optimization Algorithm for the System Outage Probability

5.3.1 Optimization Problem

In this section, the optimization problem is set up for the purpose of minimizing the system outage probability, limited by the total transmit power.

According to the TWR system, when the second user (S_2) moves, our goal is to minimize P_{out} in (5.13) with the assumption that the relay has knowledge of the location of R_2. d_1 is assumed to be the reference distance without loss of generality, and the case that R_2 is roaming is investigated. Denote the transmit powers a_1E_b and a_2E_b at S_1 and S_2 respectively for the MA phase, and the broadcasting power a_3E_b at R in the BC phase; to compare with our former work, the total transmit power from the three peer nodes is limited by $a_1E_b + a_2E_b + a_3E_b = 4E_b$. $\dot{P}_1$, $\dot{P}_2$, $\dot{P}_3$ and $\dot{P}_4$ in (5.13) can be written as (5.14)

$$\begin{aligned}
\dot{P}_1 &= \frac{1}{1+\left(\frac{\alpha}{\gamma_0}\right)^{\beta} a_1^{\beta}} \\
\dot{P}_2 &= \frac{1}{1+\left(\frac{\alpha}{\gamma_0}\right)^{\beta} (l^2)^{\beta} a_2^{\beta}} \\
\dot{P}_3 &= \frac{1}{1+\left(\frac{\alpha}{\gamma_0}\right)^{\beta} a_3^{\beta}} \\
\dot{P}_4 &= \frac{1}{1+\left(\frac{\alpha}{\gamma_0}\right)^{\beta} (l^2)^{\beta} a_3^{\beta}}.
\end{aligned} \tag{5.14}$$

Then the optimization problem can be summarized as

$$\begin{aligned} \min \quad & P_{out} \\ s.t. \quad & a_1 + a_2 + a_3 = 4 \\ & 0 \leq a_1, a_2, a_3 \leq 4 \end{aligned} \tag{5.15}$$

5.3.2 Contour Illustration for the Optimization Problem

The optimization problem summarized in (5.15) is a nonlinear transcendental function, which is too complicated to get the analytical solution. However, the objective function P_{out} is convex in its feasible regions. It can be demonstrated by the contours as shown in Fig. 5.4, representing the convexity of P_{out} under the CM1 channel environment.

5.3.3 Optimization Method for the Linear Outage Probability

To solve the optimization problem in (5.15), $\mathbf{a}_0 = [a_1^0 \ a_2^0 \ a_3^0]^T$ (e.g. $\mathbf{a}_0 = [\frac{4}{3} \ \frac{4}{3} \ \frac{4}{3}]^T$) can be initialized first in the feasible region, then the objective function can be derived in Taylor series as

$$P_{out}(\mathbf{a}^*) = P_{out}(\mathbf{a}_0) + \nabla P_{out}(\mathbf{a}_0) \cdot \delta + \ldots \tag{5.16}$$

where $\delta = [\delta_1 \ \ \delta_2 \ \ \delta_3]^T = [a_1^* - a_1^0 \ \ a_2^* - a_2^0 \ \ a_3^* - a_3^0]^T$. Thus the nonlinear optimization problem in (5.15) changes to a series of Linear Programming (LP) problems.

In the same way, for each feasible point $\mathbf{a}_k$, the LP problem can be written in a

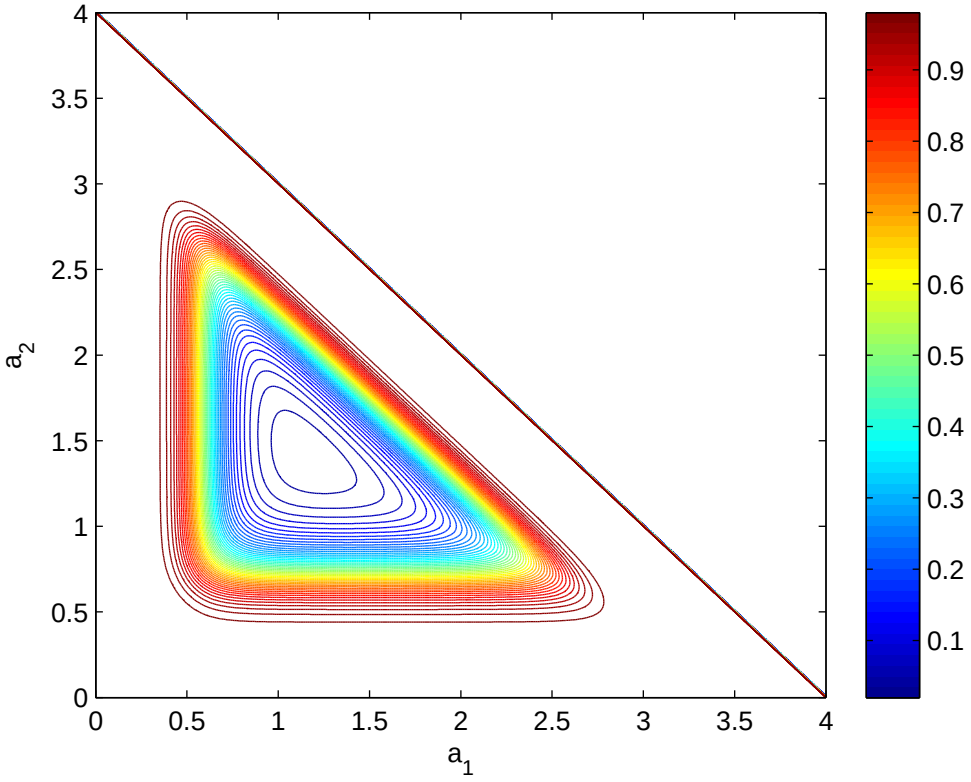

Figure 5.4: Contours for P_{out} under CM1 channel environment ($\frac{E_b}{N_0}$ =22 dB, γ_0 =30 dB and l^2 =0.8)

standard formed LP case as

$$\begin{aligned} min \quad & \left(\frac{\partial P_{out}}{\partial a_1} - \frac{\partial P_{out}}{\partial a_3}\right)|_{\mathbf{a}_k} \cdot \delta_1 + \left(\frac{\partial P_{out}}{\partial a_2} - \frac{\partial P_{out}}{\partial a_3}\right)|_{\mathbf{a}_k} \cdot \delta_2 \\ s.t. \quad & \delta_1 \geq -\tau \\ & -\delta_1 \geq -\tau \\ & \delta_2 \geq -\tau \\ & -\delta_2 \geq -\tau \\ & \delta_1 + \delta_2 \geq -\tau \\ & -\delta_1 - \delta_2 \geq -\tau \end{aligned} \tag{5.17}$$

where τ is a very small positive. The solution $\delta^* = [\delta_1^* \ \delta_2^* \ -\delta_1^* - \delta_2^*]^T = [\delta_1^* \ \delta_2^* \ \delta_3^*]^T$ is then taken back to $\mathbf{a}_k$ to get $\mathbf{a}_{k+1}$ as $\mathbf{a}_{k+1} = \mathbf{a}_k + \delta^*$. The iteration stops when $\nabla P_{out} \cdot \delta < \varepsilon$, where ε is a given small positive.

5.3.4 Algorithm for the Optimization Problem

For the LP problem as (5.17), there are several optimization methods that can be applied to get the numerical results. Since all the vertices in (5.17) are nondegenerate, the simplex method (Algorithm 11.1 in [40]) is introduced here to solve the optimization problem.

With $Q = \begin{bmatrix} 1 & -1 & 0 & 0 & 1 & -1 \\ 0 & 0 & 1 & -1 & 1 & -1 \end{bmatrix}^T = \left[\mathbf{q}_1^T \ \mathbf{q}_2^T \ \mathbf{q}_3^T \ \mathbf{q}_4^T \ \mathbf{q}_5^T \ \mathbf{q}_6^T\right]^T$, $\mathbf{b} = -\tau[1\ 1\ 1\ 1\ 1\ 1]^T$.

The steps follow:

STEP 1

Input vertex $\delta_0 = [-\tau \ \tau]^T$, δ_0 has two active constraints, as $\{ \begin{matrix} -\tau \cdot 1 + \tau \cdot 0 = -\tau \\ -\tau \cdot 0 + \tau \cdot (-1) = -\tau \end{matrix}$.

$Q_{q_0} = \begin{bmatrix} 1 & 0 \\ 0 & -1 \end{bmatrix}$, $J_0 = 1, 4$ and $k = 0$.

STEP 2

Solve $Q_{q_k}^T \mu_k = [\frac{\partial P_{out}}{\partial a_1} - \frac{\partial P_{out}}{\partial a_3} \;\; \frac{\partial P_{out}}{\partial a_2} - \frac{\partial P_{out}}{\partial a_3}]|_{\mathbf{a}_k}^T$ for μ_k. $Q_{q_k} \triangleq [\mathbf{q}_{j_1}^T \; \mathbf{q}_{j_2}^T]^T$ and $\mathbf{J}_k \triangleq \{j_1, j_2\}$, where j_1 and j_2 are the indices of the active constraints.

If $\mu_k \geq 0$, break (δ_k is a vertex minimizer);

otherwise, select index (l) corresponding to the most negative component in μ_k.

STEP 3

Solve $Q_{q_k} \mathbf{d}_k = \mathbf{e}_l$ for $\mathbf{d}_k$,

where $\mathbf{e}_l$ is the l-th column of the 2×2 identity matrix.

STEP 4

Compute the residual vector $\mathbf{r}_k = Q\delta_k - \mathbf{b} = (r_i)_{i=1}^6$.

Define Index set I_k as $I_k = \{i : r_i > 0 \text{ and } \mathbf{q}_i^T \mathbf{d}_k < 0\}$.

If I_k is empty, break (objective function in (5.17) tends to $-\infty$ in the feasible region);

otherwise, compute $\varrho_k = \min_{i \in I_k} \left(\frac{r_i}{-\mathbf{q}_i^T \mathbf{d}_k} \right)$, and record i^*.

STEP 5

Set $\delta_{k+1} = \delta_k + \varrho_k \mathbf{d}_k$.

Update $Q_{q_{k+1}} = \begin{cases} [\mathbf{q}_{j_1}^T \; \mathbf{q}_{i^*}^T]^T & l = 2 \\ [\mathbf{q}_{i^*}^T \; \mathbf{q}_{j_2}^T]^T & l = 1 \end{cases}$ and $J_{k+1} = \begin{cases} \{j_1, i^*\} & l = 2 \\ \{i^*, j_2\} & l = 1 \end{cases}$ respectively.

Set $k = k + 1$ and repeat from Step 2.

Because (5.15) is a convex problem (demonstrated from the contour illustration shown in Fig. 5.4) with only three dimensions, bruteforce might also be a practical method to allocate the transmit powers among the nodes. Results from both the simplex method and the bruteforce tend to be equal. However, when more relay

nodes come into the cooperative process, the latter one might be unfeasible because of the complexity in the calculation.

5.4 Simulation Results for Power Allocation Strategies

In this section, the simulation results for various power allocation strategies under CM1 and CM2 channels are presented. For both of the CM1 and CM2 channel environments, E_b/N_0 is set to be 22 dB at the transmitter, thus the noise-noise version in (5.6) becomes relatively small and can be neglected. The reference distance d_1 and d_2 in Fig. 5.1 is chosen to be the same without loss of generality.

Four power allocation strategies are compared: the first one is what we have done in the previous work as $a_1 = 1, a_2 = 1, a_3 = 2$; the second case is $a_1 = 3/2, a_2 = 3/2, a_3 = 1$, which strengthens the MA phase; the Even Allocation case with $a_1 = a_2 = a_3 = 4/3$; and our Optimal Allocation strategy through the SNR modeling. Each scenario is named by its corresponding $[a_1\ a_2]$ in the simulation results for short.

The comparison under the CM1 channel environment when γ_0 is set to 25 dB and 30 dB is shown in Fig. 5.5. The blue and red curves are used to represent the cases γ_0 equals 25 dB and 30 dB in the figures. Note that when $l^2 = 1$ (that is $d_2 = d_1$), the even allocation case becomes the optimal one. From the figure, it is seen that the optimal power allocation protocol gains the minimum system outage probability. When l^2 is small, that is the distance between S_2 and R is larger than that from S_1 to R, there is an obvious advantage in the proposed strategy. When l^2 gets larger, the proposed optimal power allocation strategy is still slightly better than the even allocated case, and much more reliable than the other two cases.

The simulation results under the CM2 channel environment are shown in Fig. 5.6.

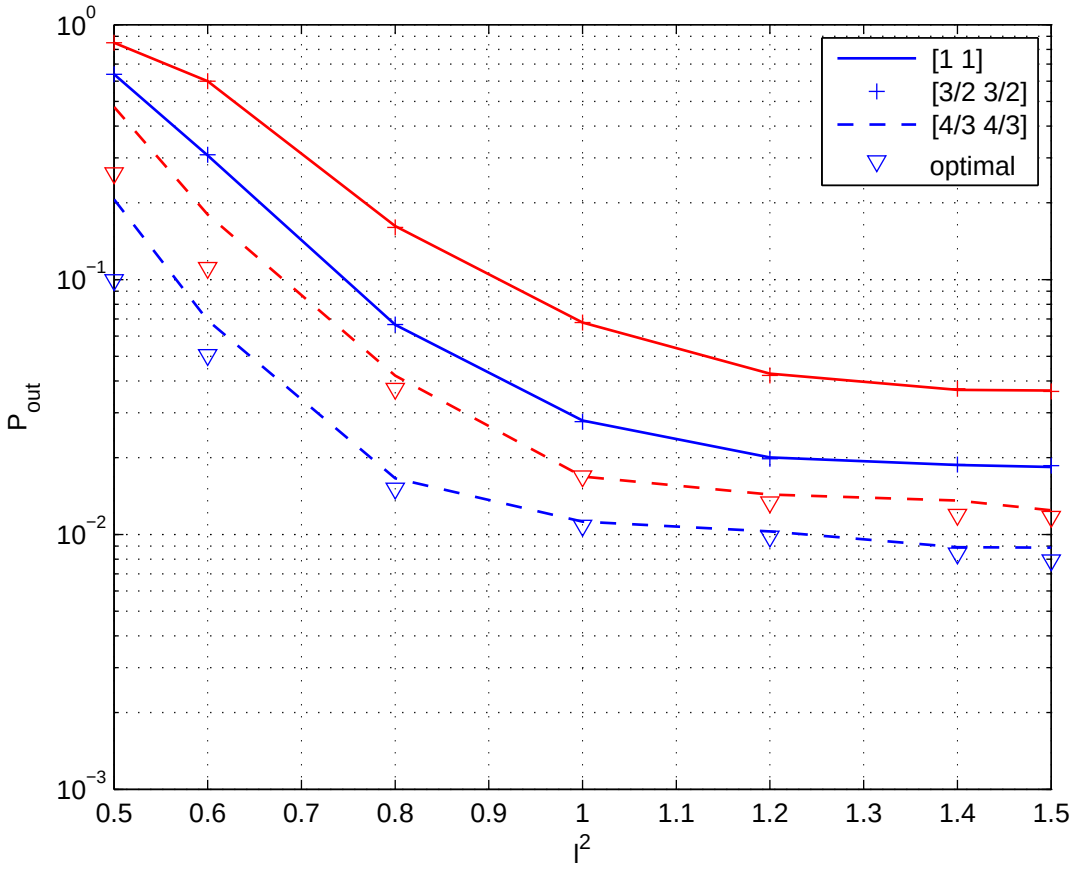

Figure 5.5: Simulation results for system outage probability under CM1 channel environment (γ_0 =25 dB and 30 dB)

It can be observed that the proposed optimized power allocation strategy shows the most robust performance when l^2 changes under the CM2 channel environment, consisting with the CM1 case.

To make the simulation results more convincible, the BER performance is also investigated for different strategies. When E_b/N_0 is 18 dB, and γ_0 equals 10 dB, the system performance are shown in Fig. 5.7 and 5.8 respectively for CM1 and CM2 channels. And the optimal power allocation strategy is also demonstrated to be the most reliable one in both cases.

The system performance will be further improved if the transmit power is allocated according to each channel realization. However, with the statistical SNR distribution model, channel estimation is no longer necessary with a penalty of loss in the system performance.

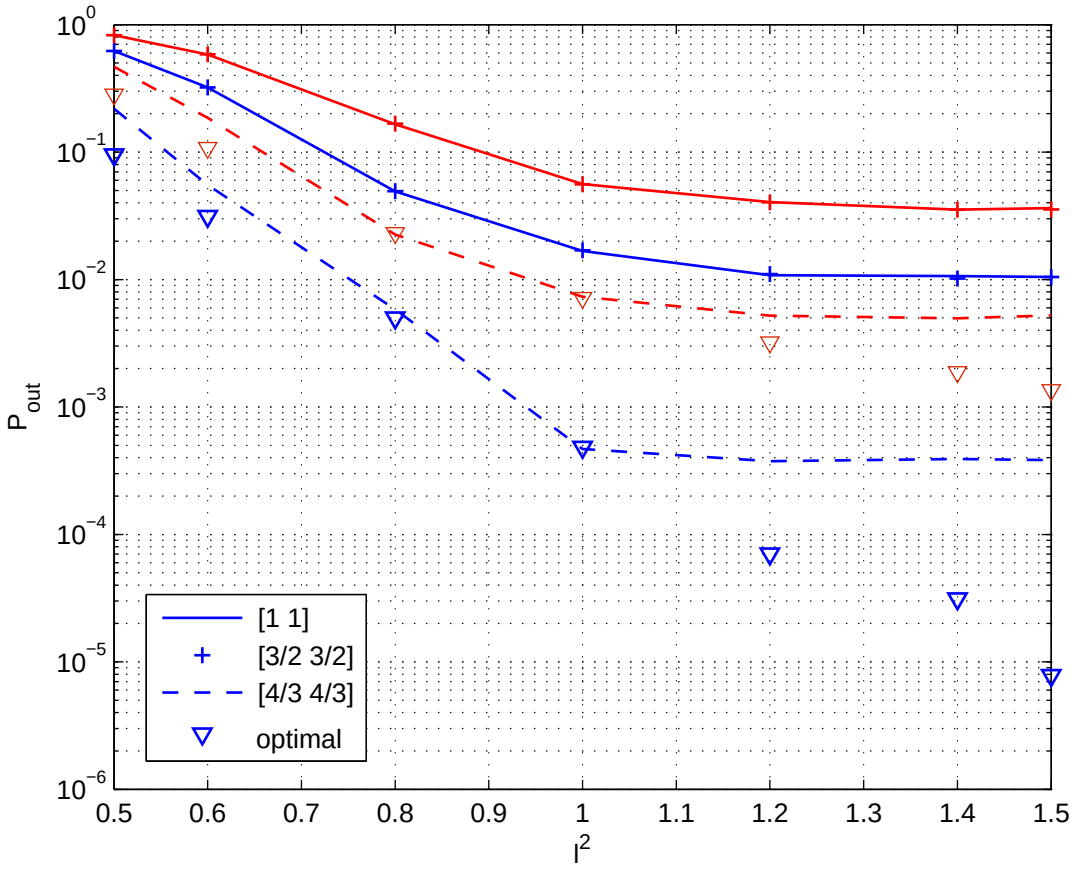

Figure 5.6: Simulation results for system outage probability under CM2 channel environment (γ_0 =25 dB and 30 dB)

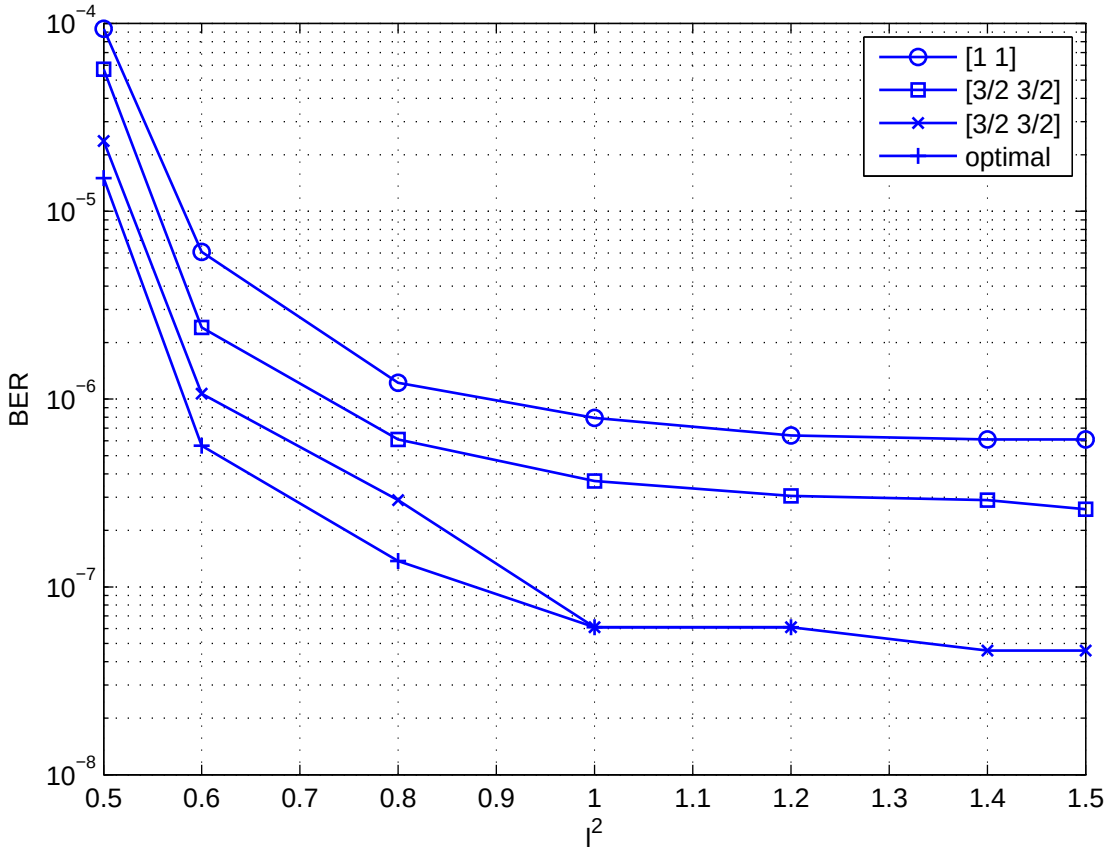

Figure 5.7: Simulation results for BER under CM1 channel environment (γ_0 =10 dB)

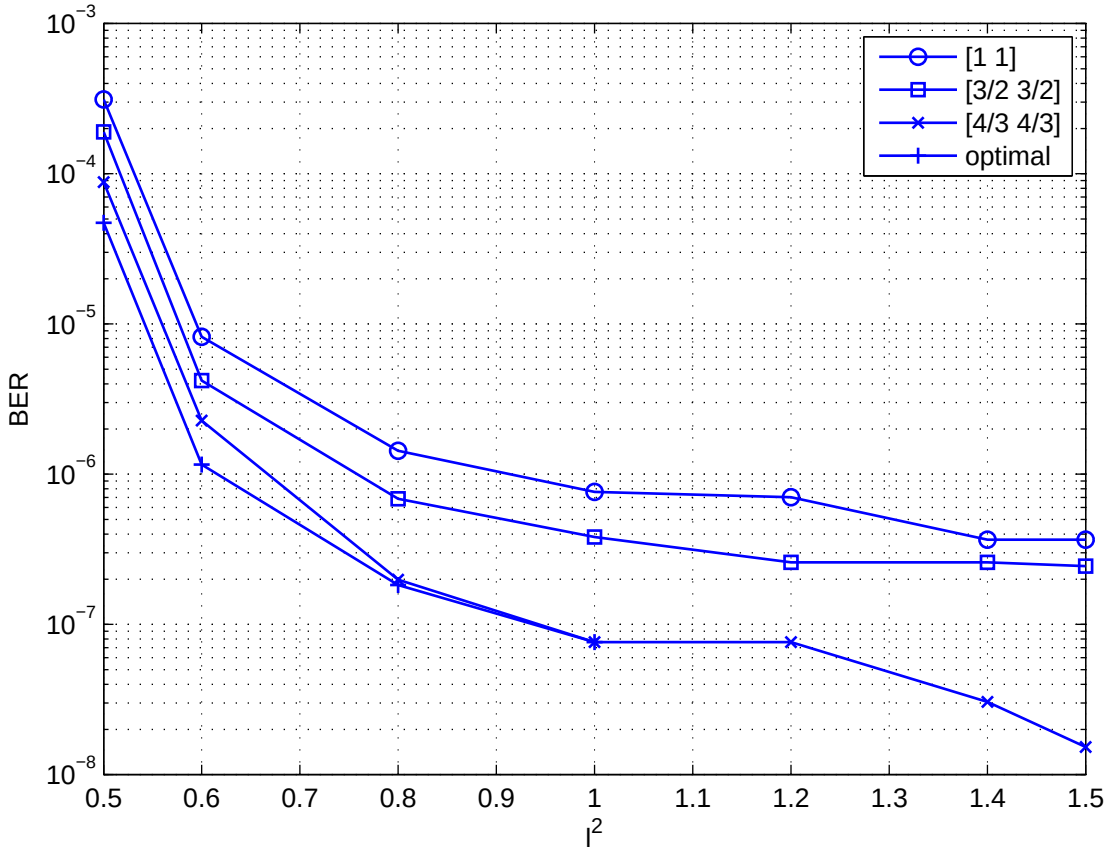

Figure 5.8: Simulation results for BER under CM2 channel environment (γ_0 =10 dB)

Chapter 6

Conclusion and Future Work

6.1 Conclusions

Ultra-wideband is a fast burgeoning technology with inviting features in wireless communications. Compared to narrow-band technologies, UWB has greater channel resolution thanks to its extremely narrow pulses. These pulses make accurate localization possible in UWB, but they also pose a tremendous challenge on the receiver design at the same time, particularly on the channel estimation. Moreover, as a short range communication technology, with transmit power strictly regulated by the spectrum governing body, a UWB network can further extend its coverage, enhance error or rate performance through the use of cooperative relays. In recent years, there are a vast amount of published work on general user cooperation and relay networks. This thesis is based on a novel transmitting pattern named transmitted reference pulse cluster, which allows a simple and robust receiver to be implemented, with symbol rate sampling and short delay lines. The TRPC is investigated in a TWR network, and the relay cooperation and power allocation strategies are proposed for such a system.

In Chapter 3, different TRPC cooperative strategies have been proposed for a bi-directional two relays UWB network with physical layer network coding. Two novel decision variable based channel quality indicators have been introduced which are used to estimate the channel conditions and relay decoding qualities. Then different relay selection strategies based on these indictors have been proposed and demonstrated to achieve improved performance over directly combining decision variables from the two relays. The cooperative relay strategies maintain the low complexity feature of TRPC with no requirement on UWB channel estimation.

The shadowing effects on the cooperative systems have been investigated in Chapter 4. In the cooperative network under CM1 shadowing channel environment, the bit-by-bit relay selection strategies proposed in Chapter 3 are demonstrated to result in improved performance from simulation. And for the CM8 channel environment where shadowing is extremely heavy, the idea of multipath channel based relay selection is introduced, where channel selection is executed once for each channel realization instead of the bit level. The system performance following the channel based relay selection strategy is demonstrated to approach that of the bit-by-bit selection case, with a huge saving of the receiver overhead. Furthermore, a new JRS strategy is introduced, giving a balance on both hardware implementation and system performance.

In Chapter 5, based on the Monte Carlo experiments for CM1 and CM2 channels using TRPC, the SNR distribution models are derived. Then, the approximated SNR distribution models are further elaborated when different pathloss coefficients are taken into consideration. Straightforwardly, the outage probability function, which can be inferred from the elaborated SNR distribution model, is built for the whole TWR system. In addition, numerical optimization algorithm has been provided to find the appropriate power allocation strategy, which could result in the system's min-

imum outage probability. Extensive simulation has been executed for the proposed power allocation strategy, and numerical results have validated its effectiveness and reliability.

6.2 Future Work

1. In this thesis, a two relays cooperative bi-directional network is investigated. The source nodes exchange information with the help of the relays according to different cooperative strategies. However, in the wireless network nowadays, more peer nodes may be present in the network. Thus, cooperative strategies can be developed for network topologies incorporating more source and relay nodes.

2. For the cooperative relay strategies in this thesis, the simulation is done under the CM1 (LOS) and CM8 (NLOS) channels. For the power allocation schemes, only the CM1 and CM2 channel environments are investigated. As well, all the four hops in the cooperative network model are assumed to be under the same channel type. However, this is not always the case in reality. Other channel environments should be considered, and the scenarios that different hops in the network are under different channel environments should be investigated as well.

3. For the power allocation strategy investigated in Chapter 5, the system model is simplified into a TWR network compared with that in Chapter 3 and 4. The power allocation strategy can be extended to a more general multi-node system in the future work.

Bibliography

[1] X. Dong, L. Jin, and P. Orlik, "A new transmitted reference pulse cluster system for uwb communications," *IEEE Transactions on Vehicular Technology*, vol. 57, pp. 3217 –3224, September 2008.

[2] A. Antoniou and W. Lu, *Practical Optimication: Algorithms and Engineering Applications*. Springer.

[3] "First report and order: in the matter of revision of part 15 of the commissions rules regarding ultra-wideband transmission systems," tech. rep., FCC, April 2002.

[4] "Devices using ultra-wideband (uwb) technology," tech. rep., RSS-220, Spectrum Management and Telecommunications, March 2009.

[5] J. H. Reed, *An Introduction to Ultra Wideband Communication Systems*. Prentice Hall, June 2005.

[6] R. A. Saeed, S. Khatun, B. M. Ali, and M. A. Khazani, "Performance of ultra-wideband time-of-arrival estimation enhanced with synchronization scheme," *IEEE Transactions on Electrical Eng., Electronics, and Communications*, vol. 4, pp. 78–84, February 2006.

[7] L. Yang and G. Giannakis, "Ultra-wideband communications: an idea whose time has come," *Signal Processing Magazine, IEEE*, vol. 21, pp. 26 – 54, November 2004.

[8] K. W. Robbins, "Short base-band pulse receiver." United Ststes Patent 3,662,316, May 1972.

[9] T. Quek and M. Win, "Analysis of uwb transmitted-reference communication systems in dense multipath channels," *IEEE Journal on Selected Areas in Communications*, vol. 23, pp. 1863 – 1874, September 2005.

[10] R. Hoctor and H. Tomlinson, "Delay-hopped transmitted-reference rf communications," *2002 IEEE Conference on Ultra Wideband Systems and Technologies, 2002. Digest of Papers*, pp. 265 – 269, May 2002.

[11] S. Gezici, F. Tufvesson, and A. Molisch, "On the performance of transmitted-reference impulse radio," *Global Telecommunications Conference*, vol. 5, pp. 2874 – 2879, November 2004.

[12] Y.-L. Chao and R. Scholtz, "Ultra-wideband transmitted reference systems," *IEEE Transactions on Vehicular Technology*, vol. 54, pp. 1556 – 1569, September 2005.

[13] S. Franz and U. Mitra, "On optimal data detection for uwb transmitted reference systems," in *Global Telecommunications Conference*, vol. 2, pp. 744 – 748, December 2003.

[14] L. Jin, X. Dong, and Z. Liang, "Integration interval determination algorithms for ber minimization in uwb transmitted reference pulse cluster systems," *IEEE Transactions on Wireless Communications*, vol. 9, pp. 2408 –2414, August 2010.

[15] C. E. Shannon, "Two-way communication channels," *in Proc. 4th Berkelev Symp. Math. Statist. and Prob.*, vol. 1, pp. 611–644, 1961.

[16] J. Laneman, D. Tse, and G. Wornell, "Cooperative diversity in wireless networks: Efficient protocols and outage behavior," *IEEE Transactions on Information Theory*, vol. 50, pp. 3062 – 3080, December 2004.

[17] A. Sendonaris, E. Erkip, and B. Aazhang, "Increasing uplink capacity via user cooperation diversity," *IEEE International Symposium on Information Theory, 1998. Proceedings.*, p. 156, August 1998.

[18] A. Nosratinia, T. Hunter, and A. Hedayat, "Cooperative communication in wireless networks," *Communications Magazine, IEEE*, vol. 42, pp. 74 – 80, October 2004.

[19] S. Cui, A. Haimovich, O. Somekh, and H. Poor, "Opportunistic relaying in wireless networks," *IEEE Transactions on Information Theory*, vol. 55, pp. 5121 –5137, November 2009.

[20] A. Bletsas, H. Shin, and M. Win, "Cooperative communications with outage-optimal opportunistic relaying," *IEEE Transactions on Wireless Communications*, vol. 6, pp. 3450 –3460, September 2007.

[21] S. Zhang, S. C. Liew, and P. P. Lam., "Hot topic: physical layer network coding," *in Proc. 12th MobiCom*, pp. 358 –365, 2006.

[22] S. Zhang and S.-C. Liew, "Channel coding and decoding in a relay system operated with physical-layer network coding," *IEEE Journal on Selected Areas in Communications*, vol. 27, pp. 788 –796, June 2009.

[23] T. Cui and J. Kliewer, "Memoryless relay strategies for two-way relay channels: Performance analysis and optimization," in *IEEE International Conference on Communications, 2008. ICC '08.*, pp. 1139 –1143, May 2008.

[24] A. Argyriou and A. Pandharipande, "Cooperative protocol for analog network coding in distributed wireless networks," *IEEE Transactions on Wireless Communications*, vol. 9, pp. 3112 –3119, October 2010.

[25] C. Abou-Rjeily, N. Daniele, and J.-C. Belfiore, "On the amplify-and-forward cooperative diversity with time-hopping ultra-wideband communications," *IEEE Transactions on Communications*, vol. 56, pp. 630 –641, April 2008.

[26] S. Zhu, K. Leung, and A. Constantinides, "Distributed cooperative data relaying for diversity in impulse-based uwb ad-hoc networks," *IEEE Transactions on Wireless Communications*, vol. 8, pp. 4037 –4047, August 2009.

[27] T. Koike-Akino, P. Popovski, and V. Tarokh, "Optimized constellations for two-way wireless relaying with physical network coding," *IEEE Journal on Selected Areas in Communications*, vol. 27, pp. 773–787, June 2009.

[28] A. F. Molisch, K. Balakrishnan, C.-C. Chong, S. Emami, A. Fort, J. Karedal, J. Kunisch, H. Schantz, U. Schuster, and K. Siwiak, "IEEE 802.15.4a channel model - final report," tech. rep., IEEE P802.15-04-0662-00-004a, October 2004.

[29] A. Saleh and R. Valenzuela, "A statistical model for indoor multipath propagation," *IEEE Journal on Selected Areas in Communications*, vol. 5, pp. 128 – 137, February 1987.

[30] L. Jin, "The transmitted reference pulse cluster system for ultra-wideband communications," Master's thesis, University of Victoria, August 2009.

[31] V. Havary-Nassab, S. Shahbazpanahi, and A. Grami, "Optimal distributed beamforming for two-way relay networks," *IEEE Transactions on Signal Processing*, vol. 58, pp. 1238 –1250, March 2010.

[32] A. Bletsas, H. Shin, and M. Win, "Cooperative communications with outage-optimal opportunistic relaying," *IEEE Transactions on Wireless Communications*, vol. 6, pp. 3450–3460, Sep. 2007.

[33] I. Oppermann and J. Iinatti, *UWB Theory and Applications*. Wiley, 2004.

[34] I. Guvenc, C. Chong, and F. Watanabe, "Nlos identification and mitigation for uwb localization systems," in *Wireless Communications and Networking Conference*, pp. 1571 –1576, March 2007.

[35] A. Molisch, D. Cassioli, C.-C. Chong, S. Emami, A. Fort, B. Kannan, J. Karedal, J. Kunisch, H. Schantz, K. Siwiak, and M. Win, "A comprehensive standardized model for ultrawideband propagation channels," *IEEE Transactions on Antennas and Propagation*, vol. 54, pp. 3151 –3166, November 2006.

[36] J. Karedal, S. Wyne, P. Almers, F. Tufvesson, and A. Molisch, "Uwb channel measurements in an industrial environment," in *Global Telecommunications Conference*, vol. 6, pp. 3511 – 3516, 2004.

[37] F. Haroon, H. Rasheed, and K. M. Ahmed, "An adaptive srake reception of biorthogonal ir-th uwb signals in ieee 802.15.4a industrial nlos environment," in *2010 IEEE International Conference on Wireless Communications, Networking and Information Security (WCNIS)*, pp. 237 –241, June 2010.

[38] Z. Liang, X. Dong, and T. A. Gulliver, "Adaptive decision threshold optimization for transmitted reference pulse cluster,"

[39] A. Papoulis, *Probability, Random Variables, and Stochastic Processes, 3rd ed.* New York: McGraw-Hill, 1991.

[40] A. Goldsmith, *Wireless Communications*. Stanford University, 2004.